Two dimensional modeling of sediment dynamics in braiding rivers

I. Rifai








MASTER'S THESIS

Two Dimensional Modeling of Sediment Dynamics in Braiding Rivers

Author: Ismail Rifai*

✉ ismail.rifai@irstea.fr

This study was funded by the ALCOTRA European project RISBA.

Supervisors :

Mr. Alain Recking*
Ms. Caroline Le Bouteiller*

* : *IRSTEA, UR ETNA, Saint-Martin d'Heres, France*

Grenoble, July 2014

Acknowledgment

I would like to thank my supervisor M. Alain Recking for accepting me as a trainee at IRSTEA of Grenoble, for providing me the necessary facilities to work on my master's thesis, and above all, for the great opportunities he gave me to expand my experience in the field of research.

I also express my sincere gratitude to Ms. Caroline Le Bouteiller for her patience, the time spent for my concern, her thorough advice, for providing valuable answers to my frequent questions and her appreciation of my work.

I also thank M. Guillaume Piton for the literature he recommended, his constructive instructions, his help in flume experiments and especially the assistance he offered during my first days in Grenoble.

And I place on record my sincere thanks to the other interns, with whom I had a great time, for their help and support.

أخيرا، أود أن أشكر أمي، أبي وأسرتي لما قاموا به لأجل إرضائي وسهرهم على توفير كل ما بوسعهم لتيسر مساري الدراسي.
هذا التقرير مهدا لهم.

Ismail Rifai

Abstract

Braided rivers are self-induced forms of alluvial streams which are characterized by a multichannel network separated by ephemeral exposed bars. Prevailing sediment inflow, high stream power and erodible banks are necessary conditions for braiding. The complicated pattern of braided streams and their high dynamics make them challenging for both understanding and modeling. Several modeling works have been conducted in the case of braiding rivers. Here we investigated the robustness of a physical based 2-D model (TELEMAC2D coupled with SISYPHE) and its ability to reproduce the braiding dynamics from the initiation, starting from an initially flat bed with a central incision, to the evolution of the pattern resulting from different flow and sediment forcings and different sediment transport formulas. The idealized river model remained close, dimensionwise, to flume experiments. The boundary conditions of the simulation were chosen to reproduce braiding circumstances. The fact that, on the one hand, the initial condition was a flat bed and, that on the other hand, the choice of boundary conditions was taken as simple as possible, allows to state that the resulting landform is self-induced and therefore permits to directly link the result to the constitutive relations used. This permits an isolated analysis of the model capability to reproduce the morphology and the dynamic characteristic of braided streams.

The 2-D simulations were performed using the finite element method for the hydrodynamics and the finite volume method for the morphodynamics. The scheme used for the advection of velocities and water depths were, respectively, the method of characteristics scheme and the mass-conservative distributive PSI scheme, in agreement with the default numerical parameter of TELEMAC. The bed slope effect, the deviation of the solid transport and secondary currents were also taken into account.

The simulation results showed that the TELEMAC2D/SISYPHE model was able to successfully reproduce the initiating phase of the braiding pattern. The resulting landform was comparable to flume experiment results.

The formation dynamics and bar shape compared well with those observed in both flume experiments and natural rivers. Nevertheless, passing the formation phase, the braiding pattern was not maintained and gradually tended to meander. This tendency of the system to converge to a single channel configuration might be explained by the lack of lateral variation of the inflow but also suggests processes controlling the bars and bank erosion may not be adequately represented and/or damped by the mesh's level of refinement.

Résumé

Les rivières en tresses sont des cours d'eau présentant plusieurs chenaux qui se divisent, s'entrecroisent et se rejoignent. L'abondance de l'apport en sédiments, une puissance forte et des berges facilement érodables sont des conditions nécessaires au tressage. Dans ce travail, nous avons cherché à évaluer la robustesse d'un modèle 2-D à base physique (TELEMAC2D couplé à SISYPHE) et juger son habilité à reproduire la dynamique de tressage ainsi que l'évolution du motif résultante de différents forçages. La construction du modèle a été largement inspirée d'expériences en canal. Ce choix a été motivé par la disponibilité de données et de points de comparaison. De plus, le fait de prendre comme état initial un fond plat et des conditions aux limites les plus simples que possible, nous a permis de mener une analyse isolée de la capacité du modèle à reproduire un motif de tresses et maintenir son développement.

Les résultats des simulations ont montré que le modèle TELEMAC2D/SISYPHE a permis de reproduire avec succès la phase initiation du motif de tressage. Le relief obtenu était comparable aux motifs des modèles physiques de tresses. En effet, la dynamique de formation des tresses et la formes des bancs est similaires à celles observées pour des rivières naturelles et bancs d'essais. Néanmoins, une fois les tresses formées, elles ne sont plus maintenus et le modèle converge vers une morphologie à chenal unique. Cela suggère un manque de variabilité latérale de l'afflux liquide et solide et/ou une mauvaise représentation des processus d'érosion des berges due à un raffinement insuffisant du maillage.

Contents

Acknowledgment **i**

Abstract **iii**

Résumé **iv**

List of Figures **xi**

List of Tables **xiv**

Notations **xv**

1 Introduction and State of the Art **1**

1.1 Introduction 1

1.2 River hydraulics and sediment transport 2

1.2.1 Hydraulics 2

1.2.2 Sediment transport in rivers 2

1.2.3 Bed load transport 2

1.3 Morphodynamics 4

1.3.1 Morphologic changes due to anthropogenic influences 4

1.3.2 Slope and width 5

1.4 Channel types 5

1.5 Numerical modeling and morphodynamic models' state of the art 5

1.6 Why TELEMAC? 7

1.7 TELEMAC-Mascaret modeling system 8

1.7.1 TELEMAC-2D 8

1.7.2 SISYPHE 9

1.7.3 Parallel simulation 9

2 Dynamics of Braided Streams **11**

2.1 Braiding water streams 11

2.1.1 Origin of braiding 12

2.1.2 Braiding rivers' particularities . . . 13
2.1.3 Braided rivers' components . . . 14
2.1.4 Morphological changes . . . 14
2.1.5 Morphometric parameters . . . 16
2.2 Flume experiments . . . 17
2.2.1 Material and methods . . . 18
2.2.2 Results . . . 18
2.2.3 Purposes and limitations . . . 20
2.3 Conclusion and recommendations . . . 21

3 Numerical Experiment **23**
3.1 Modeling with TELEMAC-Mascaret system . . . 23
3.1.1 The geometry . . . 23
3.1.2 The mesh . . . 24
3.1.3 Modeling organization . . . 25
3.1.4 Initial conditions . . . 25
3.1.5 Boundary conditions . . . 25
3.1.6 Modeling parameters . . . 26
3.2 Results presentations' plan and expected results . . . 28
3.3 Results . . . 28
3.3.1 Establishment of the braiding pattern(*Run 0 and Run 00*) . . . 28
3.3.2 Erosion (*Run 01*) . . . 34
3.3.3 Aggradation (*Run 02*) . . . 36
3.4 Additional results . . . 37
3.4.1 Variation of the water inflow . . . 38
3.4.2 Ashmore and Van Rijn . . . 38
3.4.3 Widening of the domain and slope change . . . 38
3.4.4 Sediment grading effects . . . 39

4 Discussion and conclusion **41**
4.1 Discussion of the results . . . 41
4.2 Conclusion . . . 45

Bibliography **47**

Appendixes **51**

A DEM extraction with photogrammetry method **51**
A.1 Photogrammetry . . . 51

A.2 Agisoft Photoscan 51
A.2.1 Principles 51
A.2.2 Results and Bias 52
A.3 Recommendations 53

B Steering files **55**
B.1 TELEMAC-2D steering file 55
B.2 SISYPHE steering file 56

C Simulation results **59**

List of Figures

1.1 Resurrection River, Kenai Peninsula, Alaska (from uoregon.edu) 1

1.2 Different transport modes 3

1.3 Lane's balance (Lane, 1955), taken from www.ouvrage.geni-alp.org 4

2.1 Waimakarini River, New Zeland (Google Earth) 11

2.2 Different channel types according to Schumm (1985) 12

2.3 Two modes of braiding initiation (from Ashmore (2009)) 13

2.4 Braiding occuring at the high slope segment (Yalin, 1992) 13

2.5 Change of width-depth ratio with slope Schumm and Khan (1972) 14

2.6 The pattern's change of the Isar in Geretsried resulting from the construction of a dam upstream the showed area (Malavoi and Bravard, 2010) 15

2.7 Local conversion of the channel type from meandering braiding due to the sudden widening of the valley, b. and from braiding to meandering due to the narrowing of the valley (Andes, Bolivia from Malavoi and Bravard (2010) and Google Earth) 15

2.8 Typical transect of a braiding stream model, the red lines represent the channel widths considered as active (not drawn to scale) 17

2.9 The adjustment of the bed topography, the dry areas are flattered 17

2.10 Sketch of the flume, the inflow comes from the U shaped hole 18

2.11 Bed evolution in *Run 5*. Due to grain sorting effect, the bars, light colored, are noticeable and the braiding pattern is quite visible. (The partial photographs of the flume were merged using Agisoft Photoscan) 19

2.12 Grain sorting in flume experiment, a. the coarse fraction of sediments (light colored) is located at the front of bars, b. the scouring hole turbulences wash away the fine sediments and leaves the coarse sediments 20

2.13 Bed elevation at the end of the Run 5 after the increase of the inlet flow rate 20

3.1 The model's geometry 24

3.2 Simulation organisation 25

3.3 Motion of sediment on a sloping bed. Where ψ is the flow angle and β the slope angle (Soulsby, 1997) 27

3.4 Bed evolution through time (*Run 0*) 29

3.5 The formation of bars, a. the bed's topography (*Run 0*), b. cross section of the bed, in red the cross section of a bar and in blue the cross section of a scour hole 29

3.6 Velocity field (*Run0*) . . . 30
3.7 Resulting bed topography at the end of *Run 0* (02:13:00) . . . 30
3.8 Data extraction zone with a structured grid . . . 31
3.9 Evolution of the BRI and active-BRI of $Run\ 0-00$ . . . 31
3.10 Evolution of the slopes of $Run\ 0-00$ . . . 32
3.11 Diagrammatic profiles of the bed's evolution (Leopold and Wolman, 1957) . . . 32
3.12 Evolution of the bed's volumes of $Run\ 0-00$ . . . 33
3.13 Evolution of bedload rates at different transects in $Run\ 0-00$ . . . 33
3.14 Water's velocity field vs. bedload transport rate. The channel's activity is limited to a narrow band along one to two channels. . . . 34
3.15 Evolution of the BRI and active-BRI (Run 01 starts at 02 : 15) . . . 34
3.16 Evolution of the slopes (Run 01 starts at 02 : 15) . . . 35
3.17 Evolution of the bed's volumes (Run 01 starts at 02 : 15) . . . 35
3.18 Evolution of the bedload rates at different transects (Run 01 starts at 02 : 15) . . . 36
3.19 Evolution of the BRI and active-BRI (Run 02 starts at 02 : 15) . . . 36
3.20 Evolution of the slopes (Run 02 starts at 02 : 15) . . . 37
3.21 Evolution of the volumes (Run 02 starts at 02 : 15) . . . 37
3.22 Evolution of the bedload rates at different transects (Run 02 starts at 02 : 15) . . . 37
3.23 Water velocity field of the after 3 hours, a. with random variation of the inflow velocity vectors, b. with a a constant direction of the inlet's water velocity vectors . . . 38
3.24 Elevation of the bed resulting after 3 hours with a. Van Rijn (1984) transport formula and b. Ashmore's (1988) . . . 38
3.25 Bed's elevation. The morphological changes clearly shows the influence of the initial slope 39
3.26 a. Bed's elevation of the bimodal material model after 3 hours, b. the velocity field, c. the grain sorting . . . 39

4.1 Comparison of the braiding indices (Ashmore, 1991) of the three runs . . . 42
4.2 Bedload rate for the first two hours at the section A of the model according to different formulas . . . 42
4.3 Possible (*blue*) and impossible (*red*) channels' cross sections (a., b. and c.) and the free surface (d.,e. and f.) . . . 43
4.4 a. Transition from a braiding pattern to a single-thread channel caused by the vegetation of the floodplain (Tal and Paola, 2010), b. Similar transition observed in the Run 02 (the choice of colors only serves illustrative purposes) . . . 44
4.5 Example of mesh adaptation process. a. the initial mesh with constant nodes' spacing (9536 nodes and 18632 elements), b. the detection of high bed's variation areas, c. adapted mesh to the bed's relief with a high resolution in sloping zones (7626 nodes and 14987 elements) . . . 45

A.1 3-D model of braiding bed of the flume experiment generated by Agisoft PhotoScan . . . 52
A.2 Example of a distortion of the bed (the 3-D model is curved which doesn't correspond to the reality) . . . 52

C.1 $Run\ 0-00$: Bed evolution of the bed through time 59
C.2 $Run\ 0-00$: Flow velocity evolution through time 59
C.3 Run 01: a. Bed evolution of the bed through time, b. Flow velocity evolution through time 60
C.4 Run 02: a. Bed evolution of the bed through time, b. Flow velocity evolution through time 60

List of Tables

1.1 Different numerical models for braiding rivers 6

2.1 Mixture's characteristics, $\sigma = \frac{1}{2}(\frac{D_{84}}{D_{50}} + \frac{D_{50}}{D_{16}})$ is the grading coefficient 18

3.1 Count of the domain's nodes and edges 24
3.2 Boundary conditions for each run 25

Notations

BRI	Bed Relief Index [L]
$active-BRI$	Active Bed Relief Index [L]
D_*	Particle diameter [L]
D_{50}	Median grain diameter [L]
g	Acceleration of gravity [L/T^{-1}]
H	Water depth [L]
n	Material porosity [-]
Q_b	Volumetric bedload transport rate [L/T^{-1}]
Q_{bx}	Volumetric bedload transport rate in the X direction [L/T^{-1}]
Q_{by}	Volumetric bedload transport rate in the Y direction [L/T^{-1}]
r	Local radius of curvature [L]
s	Specific density [-]
T	Deviation coefficient [-]
U	Depth averaged horizontal velocity in the X direction [L/T^{-1}]
V	Depth averaged horizontal velocity in the Y direction [L/T^{-1}]
Z_f	Bed elevation [L]
α	Secondary currents coefficient [-]
α_{mpm}	Meyer Peter Müller coefficient [-]
β	Slope angle [-]
δ	Angle of the bedload movement to the main flow direction [-]
θ'	Shields parameter [-]
$\theta_{\beta c}$	Slope effect modied Shields parameter [-]
θ_c	Critical Shields parameter [-]
θ_p	Bed-shear velocity related to grains [-]
ν	Kinematic viscosity coefficient [L^2/T]

ρ	Water density [ML^{-3}]
τ_x	Bottom shear stress component in the X direction [MLT^{-1}]
τ_y	Bottom shear stress component in the Y direction [MLT^{-1}]
Φ_b	Non dimensional bedload [-]
ϕ_i	Angle of repose of sediment [-]
ψ	Angle of the current to the up-slope direction [-]

Chapter 1

Introduction and State of the Art

1.1 Introduction

Water systems are fully involved in the water cycle and are a main vehicle for sediments transit. Besides, water streams show large variety of channels pattern, which are the results of the prevailing conditions in which they river subsists.

Leopold and Wolman (1957) developed a classification scheme for natural water streams according to their planform. They suggested three major morphological categories: straight, meandering and braided. Among this three alluvial styles, the latter are the most dynamic systems. According to the description of Leopold and Wolman (1957), braiding river flow in multiple channels around alluvial islands (see figure 1.1). Their morphodynamics is highly influenced by the sediments availability, supply and transport.

Figure 1.1: Resurrection River, Kenai Peninsula, Alaska (from uoregon.edu)

The high dynamics of braiding rivers and their sensitivity to external factors make them a good example for modeling exercise. Indeed, on the one hand side, the modeling work will allow to assess the influence of various parameters on the morphological evolution of braiding streams and also to highlight the keys processes to braids' formation. On the other hand, the modeling can allow the evaluation of the accuracy of the sediment transport equations as well as defining the extent in which they can be considered as sufficiently representative of the reality.

The aim of this Master's Thesis is to implement a two dimensional physics based model of a braiding stream's hydro-morphodynamics. The double objective of this work is to discuss the key processes to braiding initiation and development. And also, the assessment of the model's ability to accurately represent such dynamics. The results should be compared to available literature descriptions of flume and field braiding systems dynamics.

The work presented hereafter is focused on the study of morphological evolution of a braiding stream

numerical model under the influence of different parameters (such as different boundary conditions, bedload equation, sediments' type, etc.). The numerical model implementation is inspired from prior flume experiments dimensions and parameterization, which were conducted in the wide flume at IRSTEA Grenoble. Moreover, the numerical model used to this purpose is TELEMAC-Mascaret modeling system and, especially, its two hydrodynamics and morphodynamics modules, which are respectively TELEMAC2D and SISYPHE.

Therefore, this report is organized according to the following framework: First, a general review of literature relative to sediment transport, morphodynamics and a state of the art of numerical modeling in braided rivers are introduced (*Chapter 1*). This is followed by a more elaborated description of braiding systems and their dynamics followed by a presentation of the flume experiments (*Chapitre 2*). Then *Chapter 3* presents of the numerical model and its results, which are finally analyzed and discussed in *Chapter 4*.

1.2 River hydraulics and sediment transport

In the following, a brief introduction to river hydraulics and sediment transport will be presented. The purpose is the setting up of the background concepts necessary to the understanding of this work.

1.2.1 Hydraulics

To summarize, river flows are the result of, on the one hand, gravity forces applied to the water, and, on the other hand, bed friction which tends to slow it down. Therefore, for a considered water discharge the hydrolics are function of the slope (which will impact the intensity of the gravity), the grain size and topography of the bed stream (De Linares, 2007). Rivers are open-channel flows, and more precisely, natural rivers are much than deep: the width-to-depth ratio is usually very high (Yalin, 1992). Consequently, and for the sake of simplicity, great scale flows can be treated as bi-dimensional problems (shallow flow hypothesis). Nevertheless, a three-dimensional consideration is more adequate for small scale studies and for cases with low width-to-depth ratios, in which the secondary currents may be non negligible.

1.2.2 Sediment transport in rivers

Many works have been done in order to provide a better understanding and a better quantification of the sediment dynamics in running water. Indeed, sediment movement initiates when bed shear stress exceeds a threshold value. Shields (1936) defined an non-dimensional parameter θ', known as Shields parameter, used to calculate the initiation of motion of sediments. Critical Shields θ_c parameter represent the threshold value of shear stress over which the sediments start moving. From here, one should differentiate two major transport modes: bed load and suspended load. One could also add a crossing mode: saltation, in which case the transported particle bounces in an irregular manner (see figure 1.2).

1.2.3 Bed load transport

As said before, bed load is one of the two types of sediment load. It's important, for it has a large influence on the bed forms and bed stream morphology. This explains why several bedload equations were proposed during the last decades.

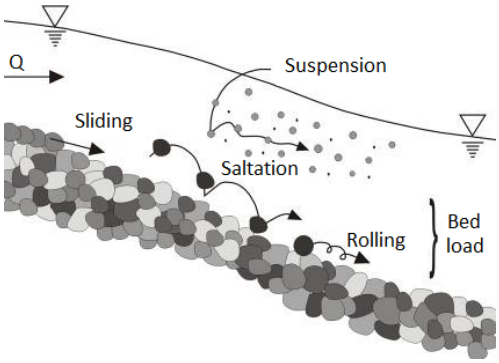

Figure 1.2: Different transport modes

Transport formulas

Many semi-empirical formulas can be found in literature. Yet, the purpose of this section is not a thorough review of developed formulas. Therefore, only the formulas which were implemented and tested in the numerical model (which is the subject of the study) were discussed hereafter. In addition, most sediment transport formulas assume a threshold conditions under which sediments are assumed to stay at rest. This is the case of all formulas considered in this study.

The following formulas give the non-dimensional sediment bedload transport rate Φ_b:

$$\Phi_b = \frac{Q_b}{\sqrt{g(s-1)D^{*3}}} \tag{1.1}$$

in which, Q_s is the volumetric bedload transport rate, g is the acceleration of the gravity, s is relative density and D^{*3} is the characteristic sediment diameter (in the following D^{*3}=D_{50}).

Meyer-Peter-Müller (1948) Meyer-Peter-Müller formula is one of the most commonly used for bed load transport rate calculation. This threshold formula has been validated for sediments in the range $0.4mm < D_{50} < 29mm$ and is based on a large data set provided from flume experiment.

$$\Phi_b = \alpha_{mpm} * (\theta' - \theta_c)^{3/2} \tag{1.2}$$

where α_{mpm} is a coefficient usually taken equal to 8, θ' is the Shields parameter and θ_c is the critical Shields parameter (in this work, and when using the Meyer-Peter-Müller formula, it will be taken equal to 0.047).

Ashmore (1988) This formula has been calibrated on data set from braiding flume experiment with varying slopes. The conducted experiments showed that bed load transport is limited to a small section of the dominant channels. In his flume experiments Ashmore (1988) considered, as being active, only the channels with a water depth greater than or equal to $2mm$.

$$\Phi_b = 3.11 * (\theta' - \theta_c)^{1.37} \tag{1.3}$$

In the following, when using this formulation of the non-dimensional sediment transport rate, the critical Shields parameter will be taken equal to $\theta_c = 0.045$. This value of θ_c gave a better fit to the experiments performed by Ashmore (1988).

Van Rijn (1984) Following the approach of Bagnold (2008) and assuming that bed load transport, under the influence of hydrodynamic fluid and gravity forces, is dominated by the saltation motion mode. He provided formulation for the bed load transport rate for particles in the rage of $0.2mm < D_{50} < 2mm$.

$$\Phi_b = 0.053 D_*^{-0.3} \left(\frac{\theta_p - \theta_c}{\theta_c} \right)^{2.1} \tag{1.4}$$

With $D_* = D_{50} \left[\frac{(s-1)g}{\nu^2} \right]^{1/3}$, θ_p is the bed-shear velocity related to grains and θ_c the critical Shields parameter.

This formula provides a reliable estimation of bed load transport rate for this range of particles and was verified using 580 data, from the field (56 tests) and flume experiments (524 tests) (Van Rijn, 1984).

1.3 Morphodynamics

To talk about morphodynamics, one should first introduce the theoretical principle of dynamic equilibrium of water streams. Indeed, Rivers tend to achieve "dynamically stable" equilibrium conciliating between two types of variables, *control* and *response* variables. This concept is schematically represented by the lane balance presented in figure 1.3. On the one hand, the control variables, as the stream flow and the sediment discharge are imposed to the system and are the result of the watershed's configuration, its hydrology, the climate and so on. These control variables are imposed to the system, which will adjust its response variables in order to reach the state of equilibrium. These response variables are therefore the local slope, the sinuosity, and the channel width among others (Malavoi and Bravard, 2010). For instance, as one can see in the Lane's balance, a decrease of the stream flow will cause an aggradation phase. Subsequently, the equilibrium will be reached by the adjustment of the slope. A higher slope will induce a higher sediment transport in order to achieve a new equilibrium state in agreement with the new control variables.

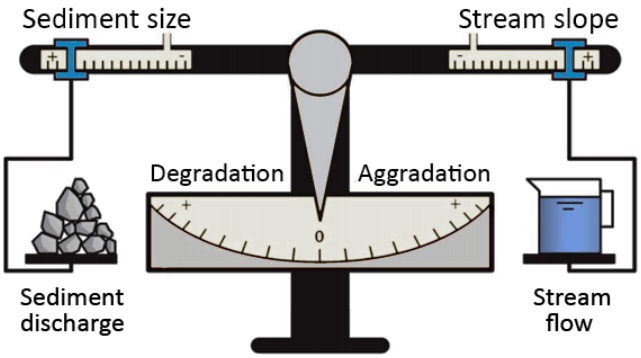

Figure 1.3: Lane's balance (Lane, 1955), taken from www.ouvrage.geni-alp.org

Nevertheless, this schematic representation (Lane balance) of water streams dynamics remains simplistic, for it does not account of other response variables such as the channel width, or more specifically its transverse geometry, nor its sinuosity, etc.

1.3.1 Morphologic changes due to anthropogenic influences

Needless to say how much the human activities have a significant impact on the environment. In particular, anthropogenic actions affecting the hydrology and sediment yield of a catchment will have inevitably an effect on the alluvial style of its watercourse.

For instance, braiding rivers (which are the subject of this work) are highly sensitive to the changes affecting sediment supply and/or flood patterns (Ferguson, 1993). On the one hand, activities that will tend to increase the sediment influx can make a different river pattern shift to a braiding scheme and conversely a drastic decrease of the sediment discharge, due to construction of a dam or major climate change for example will lead to the gradual fading of the braiding pattern to a meandering like configuration (Malavoi and Bravard, 2010; Piégay and Grant, 2009).

1.3.2 Slope and width

The slope is an important morphological parameter. It is a "response variable" (the increase of the slope is due to the system's need to ensure a higher dynamic required by the high sediment influx rate, see figure 1.3) which differentiates the resulting rivers morphology. Indeed, ceteris paribus, a meandering system will have a lower slope than a braiding one (Ashmore, 2009). Also, the width helps segregating different systems from straight, meandering, braiding river channel pattern, the latter will have the highest width to depth ratio Schumm and Khan (1972).

1.4 Channel types

Among the different alluvial rivers, and depending on their slope and morphology, one can differentiate several alluvial types. Starting from the upstream part of a water stream, the **waterfalls** are present when the slopes are high (more than 10%) and usually in confined valleys. The waterfalls can be described as an entanglement of rocks and boulders with no apparent organization. They are usually stable, even at the occurrence of floods. At lower slopes (from 3% to 10%), **step-pools** are formed with a regular succession of steps, wich can be assimilated to staircase in the bed of stream, formed with coarsest fraction of bed material interlaced with fines. And pools, which provide a storage for finer bed material.

Then, when the slope is lower (from 1% to 3%), one can encounter two alluvial styles: **alternate bars** and **braiding rivers**. Alternate bars are typically a succession of emerged sediments deposits alternating between the river's sides. The braiding rivers are formed, as their designation might indicate, (see figure 1.1) with large gravel bed in which a network of channels which dived and merge around usually temporary islands called bars.

However, one should differentiate braiding rivers from other comparable alluvial styles: **anabranch** and **anastomosis**. The first can be assimilated to a system of multiple channels characterized by alluvial islands which are vegetated and stable (Nanson and Knighton, 1996). The term anabranch refers to a stream which diverts from the main channel and rejoins it downstream. The anastomosis designates multiple channels, which are more stable than braiding rivers', more sinuous, narrower and deeper with a lower slope. This channels delimitate relatively steady and large islands (Malavoi and Bravard, 2010).

Finally, for even lower slopes and finer sediments, one encounters **meandering** and **straight** channel patterns.

The braiding rivers are the main interest of this work and are presented in more details in the next chapter.

1.5 Numerical modeling and morphodynamic models' state of the art

In order to understand, quantify and predict rivers behavior and changes, several numerical models were developed. Depending on the scale, in time and space, of the study, different approaches can be

considered, and in that sense, each model will reveal its strengths and weakness. In what follows, a general review of some hydro-sedimentary models will be presented. The purpose of this section is to give a global, yet not exhaustive, appreciation of existing models and the work conducted for the case of braiding systems.

Table 1.1 presents seven examples of braiding river' numerical models. The work of Jagers (2003) gave a substantial review of the different existing models. He compared different modeling approaches: neural network, branches model, cellular model and general 2/3D models (see table 1.1) and concluded that although each of these models has its strength and weaknesses, the branches and general 2/3D models seem to be the most promising.

Work	**Model**	**Scale**	**Comment**
Jagers (2003)	Delft3D + Cellular, Branches and Neural model	Different models inspired from the Jamuna River	Concluded that the branches model is the most promising. Although, a general 2D-model-based Monte Carlo simulation is an interesting development path.
Schuurman et al. (2013)	Delft3D	80 km x 3.2 km and 80 km x 6.4 km	Rather realistic results. However the braiding pattern once established becomes static.
Rüedlinger and Molnar (2010)	BASMENT	Pfynwald river reach	1D simulation and 2D simulation in a smaller domain. The 1D model is not suitable for braiding configuration.
Enggrob and Tjerry (1999)	MIKE 21C	Inputs of the Brahmaputra-Jamuna river (30 yr)	2D models well predict short-term planform changes. Which is not the case for long-term simulation, due to the chaotic behavior of braiding systems.
Leduc (2010)	RUBAR 20	Bés	Several limitations such as the uncoupling of hydrodynamics with bed-load transport, the rectangular meshing inhibits the cross-flows.
Ziliani et al. (2013)	Caesar RCM	33 km of Tagliamento River over 8 years	Good computational performances of the Reduced Complexity Model but gives a poor reproduction of the braided channel dynamics.
Murray and Paola (1994)	Cellular model	–	Cellular model for braided streams. However, due to the simplifications, this model is not suitable for predicting planform changes of an actual river.

Table 1.1: Different numerical models for braiding rivers

The work of Schuurman et al. (2013) showed representative results of braiding emergence and formation on a physics-based 2-D model of a sand-bed river. Schuurman et al. (2013) also highlighted the importance of the bed slope and spiral flow effects (see paragraph 3.1.6.3 page 26). The 2-D depth averaged module of the morphodynamic model Delft3D succeeded on reproducing braiding rivers' characteristics such as the wave length, the bars shape and scour holes among others. However, past the near-equilibrium stage the model started showing rather unrealistic morphology: the bars become static and develop exaggerated length and height.

Rüedlinger and Molnar (2010) performed both 1-D and 2-D modeling of a braiding segment of Rhone

river. They concluded that even if the modeling of the hydrodynamics might give satisfactory results, simulating the mophodynamics with 2-D physics based model remains a difficult task for its accuracy may rely a lot on data availability. However, 1-D models do not succeed on predicting short term processes and, therefore, the result obtained by this models must be considered with additional care.

Leduc (2010) underlined several limitations of the 2-D physics based model RUBAR 20. From this work one can site the inadequacy of rectangular mesh, the uncoupling of the hydrodynamics and morphodynamics increases the instabilities and the inadequacy of the available sediment transport formulas for low depth-width ratio streams.

The two last models presented in table 1.1 are Caesar RCM , which is a Reduced complexity model, and a Cellular model. Both showed relatively good computational performances. However, Ziliani et al. (2013) and Murray and Paola (1994) observed that in the case of long-term simulations the cited models tend to lack on reproducing braiding channels dynamic. A further analysis of this "alternative" models is presented in the work of (Jagers, 2003).

To summarize, one can state that a 2/3D approach presents numerous advantages from which we can cite:

- The modeling is based on fundamental physics laws and empirical relations of sediment transport;
- The results can be as detailed as the computation performances can allow (in terms of process time and available memory space);
- The possibility to refine the mesh in areas where more precision is needed;
- Depending on one's interest, the model can be complemented with various physical processes (i.e. accounting of the slope effect, hiding-exposure factor, ...);

Despite this advantages, a conventional 2/3D model remains highly time consuming and requires more data than a branches or neural model for instance. In addition, long term simulations are subject to great incertitude in this kind of models. This latter issue can be addressed by a Monte Carlo simulation Jagers (2003). But here again, the coupling of a probabilistic approach will increase, say 100 times at least, the computation time.

Nonetheless, for the sake of this work, a 2D model proved to be adequate. On the one hand, the investigation of the braiding system response to various configurations and the effect of different transport formulas for instance can accurately be examined with a 2D model. On the other hand, the choice of a 2D rather than a 3D consideration is justified by both the shallowness of braiding pattern and the scale in which the problem is discussed (a global appreciation of the braiding pattern formation and evolution).

Table 1.1 presented several numerical models that have been used in the case of braided rivers. To the best of our knowledge, no work was conducted with TELEMAC-Mascaret modeling system (see paragraph below). The following modeling work will be conducted using this modeling system. The next section of this chapter will therefore be dedicated to its presentation.

1.6 Why TELEMAC?

Among other sets of solvers, the TELEMAC-Mascaret system presents many interesting features. First, TELEMAC-Mascaret suit of solvers is open source and therefore free to use. Secondly, it can be described as flexible, for it offers a rather easy access to all the subroutines that intervene throughout the problem resolution. Finally, it can be used in parallel form; a huge advantage in terms of reduction of computation time. A detailed description of the TELEMAC system is presented in the following.

1.7 TELEMAC-Mascaret modeling system

TELEMAC-Mascaret modeling system is an open source program developed by the Research and Development division of Electricité de France in the Laboratoire National d'Hydraulique. It's a powerful tool for free-surface flows problems modeling and is commonly used in river and maritime hydraulics. The geometry which will be considered in the models is meshed into a grid of triangular elements. It has numerous simulation modules for hydrodynamics (1D, 2D or 3D), sediment transport, dispersion and underground flow, in addition to pre and post-processors (http://www.opentelemac.org/). In this work, only the hydrodynamics and sediment transport are of interest. Therefore, only the modules TELEMAC-2D and SISYPHE will be used (see the following paragraphs).

One should also note that the TELEMAC-Mascaret modeling system, from the mathematics, the physics, to the advanced parallelisation, is written in Fortran.

One other major strength of TELEMAC is that it allows the user to implement any functions of a simulation module by modifying specific subroutines in Fortran. This makes it easy, in a way, to work with specific formulas for the sake of test and validation for example.

1.7.1 TELEMAC-2D

TELEMAC-2D code is a hydrodynamics module of the TELEMAC-MASCARET system. It solves the 2D Saint-Venant equations, or shallow water equations (Hervouet, 2007).

$$\frac{\partial H}{\partial t} + \frac{\partial HU}{\partial x} + \frac{\partial HV}{\partial y} = 0 \tag{1.5}$$

$$\frac{\partial U}{\partial t} + U\frac{\partial U}{\partial x} + V\frac{\partial V}{\partial y} = -g\frac{\partial Z}{\partial x} + \frac{\tau_x}{\rho H} + \frac{1}{H}\frac{\partial}{\partial x}\left(H\nu\frac{\partial U}{\partial x}\right) + \frac{1}{H}\frac{\partial}{\partial y}\left(H\nu\frac{\partial U}{\partial y}\right) \tag{1.6}$$

$$\frac{\partial V}{\partial t} + U\frac{\partial V}{\partial x} + V\frac{\partial V}{\partial y} = -g\frac{\partial Z}{\partial x} + \frac{\tau_y}{\rho H} + \frac{1}{H}\frac{\partial}{\partial x}\left(H\nu\frac{\partial V}{\partial x}\right) + \frac{1}{H}\frac{\partial}{\partial y}\left(H\nu\frac{\partial V}{\partial y}\right) \tag{1.7}$$

with:

H is the water depth

U and V the depth averaged horizontal velocities

g is the acceleration due to gravity

τ_x and τ_y are the bottom shear stress components

ν the kinematic viscosity coefficient

ρ the water density.

These equations are derived from equations of conservation of mass and conservation of momentum (Navier-Stokes equations).

The results provided from solving these equations are therefore water depths and the depth-averaged velocities for each node of the problem's grid.

TELEMAC-2D is a polyvalent tool, for it allows to considers several phenomenon : treatment of singularities, friction on the bed, supercritical and subcritical flows, dry areas in the computational field like tidal flats and/or flood-plains, inclusion of porosity... and, as it's the case in this work, can be also coupled with a 2D sediment transport module (SISYPHE).

1.7.2 SISYPHE

SISYPHE, as introduced before, is a sediment transport and bed evolution module. Sediment transport, both bed load and suspended, are computed at each node depending on the flow and sediment grain parameters. Once the sediment transport calculated, the bed evolution is obtained by the resolution of the bed evolution equation, also called the Exner equation:

$$(1-n)\frac{\partial Z}{\partial t}+\frac{\partial Q_{bx}}{\partial x}+\frac{\partial Q_{by}}{\partial y}=0 \tag{1.8}$$

in which:

n is the bed's sediment porosity

Z the bed's elevation

Q_{bx} and Q_{by} are respectively volumetric sediment transport rate in the x and y direction.

In SISYPHE, this equation is solved by default, whith the finite volume formulation but can be changed to finite element scheme if needed.

It should be noted that SISYPHE allows to work for a large variety of hydrodynamic conditions and can take into account several sediments transport processes such as: secondary currents, the bed slope effect, sediment deviation and tidal flats among other processes. Also, the bed shear stress can be accounted for by imposing a friction coefficient (per node) or by using a bed-roughness predictor (Sisyphe V6.3 User's Manual).

It is important to recall that TELEMAC-Mascaret modeling system allow a coupled approach between the hydrodynamics and sediment transport. A simplified approach (uncoupled mode) consists on computing the bed evolution according to the results of a prior hydrodynamic simulation. As the bed form changes, SISYPHE corrects the velocities according to simple algorithm which will insure the conservation of the lineic flow rate (Velocity × Water depth). For instance, in an erosion area the flow velocity is decreased. This simplistic methods is not suitable in the case of this work and will not allow a proper formation of a braiding pattern starting from a initially flat bed.

Conversely, the coupled mode of SISYPHE allows the consecutive calculation of both the hydrodynamics and morphodynamics. Indeed, after a certain number of time steps (set by the user) the results of the hydrodynamics, namely the nodal velocities and water depth are communicated to the morphodynamics module, the shear stress is computed and the bedfrom updated (by solving the Exner equation). The hydrodynamics of the next time step are then simulated according to the new bedform, which will be again updated according to the new morphodynamics, and so on.

The modeling work presented in the following is performed according to this approach.

1.7.3 Parallel simulation

To be brief, parallelism consists of using simultaneously cluster of computers, or a cluster of processors in the same computer, in order to solve one single problem. Ideally, the use of n processors would divide the CPU time by n (Hervouet, 2007).

TELEMAC-MASCARET system allows to run parallel simulations. In this case, working on MS Windows operating systems, it's recommended to work with MPICH2 implementation of the Message Passing Interface standard (MPI-2[1]) which is freely available.

[1] Library specification for message-passing. It's a standard application programming interface that can be used to create parallel applications.

The use of the TELEMAC-MASCARET system in a parallel form can be very practical in terms of reduction of CPU time. In addition, the fact that it is parallelised under MPI-2 makes it portable to high-performance computing infrastructure.

☞ **Remark**: In some cases, the speed factor (the ratio between the CPU time of a simulation performed on a single processor and the CPU time when the same simulation is run with multiple processors), can turn out to be higher than the number of processors used. This happens when the memory size inhibits the efficiency of the processor when the number of elements in the whole mesh is really high (Hervouet, 2007).

Chapter 2

Dynamics of Braided Streams

The aim of this chapter is to give a more elaborated presentation of braiding streams and also to set up the required basis to the understanding of the work covered in this report. To do so, the first section will deal with the dynamics and specificities of braiding systems. It will be followed by a presentation of some of the morphometric parameters which will be used in the next chapter. Also, a flume experiment on braiding rivers will be discussed in the light of some similar work in literature.

2.1 Braiding water streams

Braided rivers can be described as a network of small channels separated by ephemeral exposed bars (Ashmore, 2009). Yalin (1992) defines the braiding process and a "self-induced" form and an ongoing response to prevailing discharge (see figure 2.1) , valley gradient, and sediment flux (Ashmore, 2009). Usually, both the sediment supply and transport are high in braided patterns and the land-forms are sloping (Leduc, 2013; Ashmore, 2009).

Figure 2.1: Waimakarini River, New Zeland (Google Earth)

Among the existing channel types of alluvial rivers, the braiding streams are of the less stable and the more active in terms of sediment transport, or more specifically, bedload transport. Indeed, Schumm (1985) gave a classification of the channel types according to their stability, prevailing sediment transport mode and channel pattern (see Figure 2.2). The classification of Schumm (1985) associate the braiding pattern to an unstable stream with coarse sediments, a large sediments load, a high flow velocity and high stream power.

Indeed, braided rivers are particular in terms of their morphodynamics. Formed with a large gravel bed in which multiple channels cross and split; their global aspect is similar to braids. Their crossing channels are separated with gravel bars, which are very dynamic. Although, the channels can be slightly sinuous, they generally follow the orientation of the valley.

Other aspect of braided rivers, the pattern or the bed form might seem chaotic and complex. Nevertheless, and most of the time, the water flows only on half the channels (Ashmore, 2009). Also, the solid transport activity is limited to a narrow strip in the main channels (Ashmore et al., 2011).

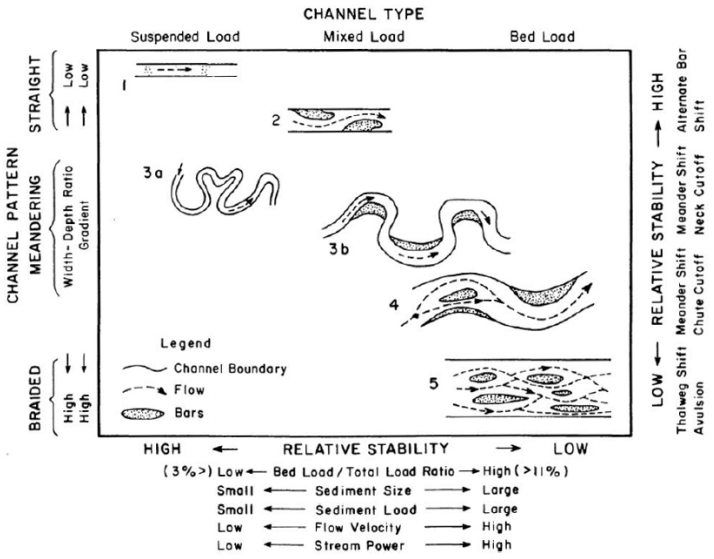

Figure 2.2: Different channel types according to Schumm (1985)

The braiding rivers can have their pattern drastically changed after the occurrence of a flood. For instance, up to 60% of the width for a morphogenetic flow in the case of Tagliamento river in Italy (Bertoldi et al., 2010).

This particularities and changes are the results of the *control* variables, or in more general terms, the conditions in which the braiding rivers subsists.

2.1.1 Origin of braiding

The reasons which lead to the initiation of the braiding of a stream are partially known. However, there is no scientific consensus yet. As cited in "Elements d'hydromorphologie fluviale" (Malavoi and Bravard, 2010), one can consider two main reasons for both the initiation and the development of braiding : an abundant bed load and easily erodible banks. The overloads encourage the first sediment deposition so as it initiate the formation of the first central bar which will cause the deflection of the flow (Leopold and Wolman, 1957) and therefore the erosion of the banks and widening of the mean stream bed (see figure 2.3).

However, this is not the only way a braiding pattern can initiate. In some cases the braiding initiates in a different way, for example by starting by developing alternate bars (Ashmore, 2009). In this case, the alternate bars will lead to the widening of the stream and the sinuosity to increases. Passing a threshold sinuosity a new bifurcation is created (Bertoldi et al., 2009).

In addition, other factors can contribute to the establishment of a braided pattern. The stream slope has an important impact on the transport rate. Thus, one should keep in mind that the slope is a consequence of the control variables. Accordingly, it will be more adequate to say that a high stream power, which is $\Omega = \rho g Q S$, is an important parameters for braiding (Malavoi and Bravard, 2010). In order to erode it shorelines and maintain its dynamics, a braided river requires a high power (see figure 2.4).

Furthermore, turbulence and the regime tendency to lower its Froude number can also be considered as factors for, respectively, initiating and developing the braiding pattern (Yalin, 1992). The fast morphological changes that the braiding river will encounter will inhibit both vegetation growth and resulting consolidation of the bars (Jagers, 2003). Conversely, a prevailing vegetation will lead, in the long term, to the transition to a dominant single-thread channel (Tal and Paola, 2010).

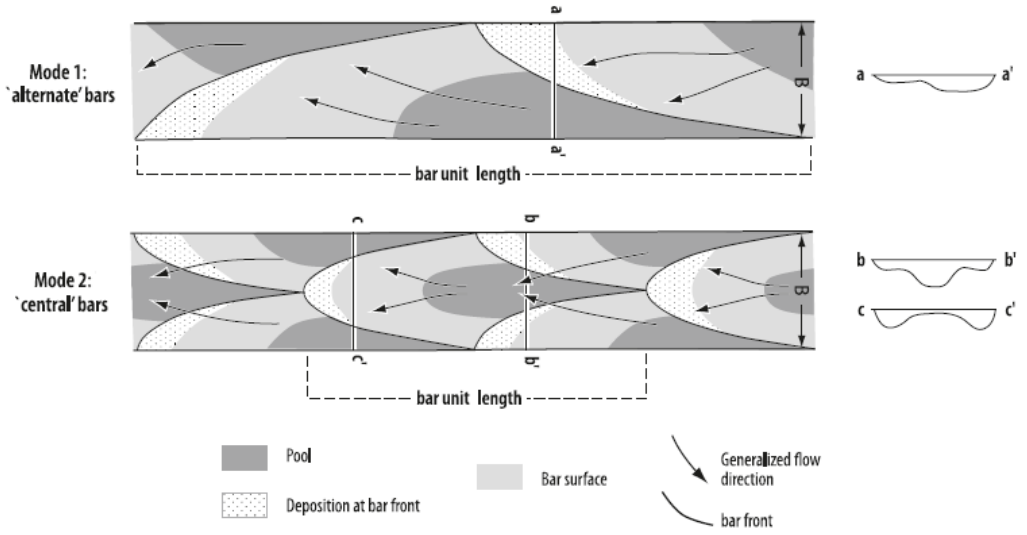

Figure 2.3: Two modes of braiding initiation (from Ashmore (2009))

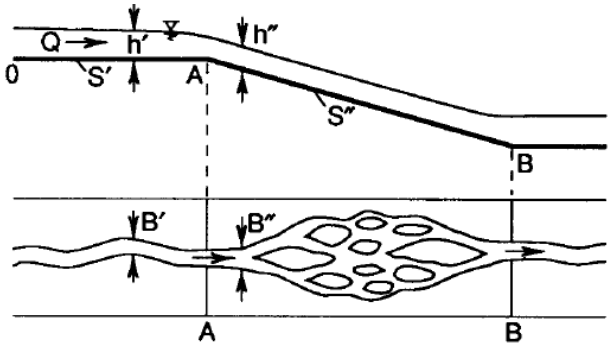

Figure 2.4: Braiding occuring at the high slope segment (Yalin, 1992)

2.1.2 Braiding rivers' particularities

As said before, braided rivers are characterized by a number of channels separated by small islands or bars and their pattern is highly mobile and changing. Yet, despite its constant and rather chaotic dynamics, a braiding river has its own particularities and morphometric characteristics.

2.1.2.1 Width - depth ratio

A braided river is wide, shallow, steep (Leopold and Wolman, 1957) and its channels move in a horizontal motion. This is therefore reflected in the fact that, for a same morphogen flow rate, a braided river will be from 5 to 10 times wider than a single channel river (Malavoi and Bravard, 2010). Also, this is clearly shown in the experimental work of Schumm and Khan (1972) (see figure 2.5). The transition from a meandering pattern to a braided channel occurs by an increase of the width-depth ratio. In some contexts, this can be seen as problematic; considering the fact that the shallowness of the channels makes almost not navigable and the frequent changes that it encounters make it hard to define a proper navigable channel.

2.1.2.2 Rectilinear braidplain

In order to increase its slope, a braided river usually follows a rectilinear path (Malavoi and Bravard, 2010). The sinuosity coefficient P (the ratio of the general axis of the stream to the valley's axis), which

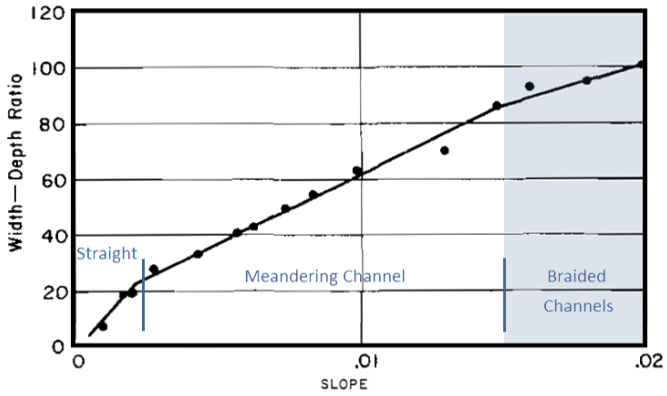

Figure 2.5: Change of width-depth ratio with slope Schumm and Khan (1972)

defines the sinuosity of a stream, is therefore low for braided rivers (lower than 1.1). Nevertheless, the sinuosity index of each channel taken apart is higher.

2.1.2.3 Active channels

Even though the braiding pattern seems very complex, studies confirm that only a fraction of the wetted width of the river is actually responsible for most changes (Ashmore et al., 2011; Tobias Gardner, 2009). In addition, in most braided rivers, one can notice one or two dominant channels which are responsible for the most morphologic changes and which and remains wetted at low water. Furthermore, a highly dominant and sinuous active channel might indicate the transition of the braided river to a wandering then a meandering pattern (Malavoi and Bravard, 2010).

2.1.3 Braided rivers' components

A braided river gathers several elements which are specific to it; and therefore, determine its specific terminology. Active channels are channel in which the bed load transport occurs. Therefore, the active width is the sum of these active channel widths. The braidplain is the width in which the braiding evolves. Nodes are the located scouring areas with high depths and the bars are sediment deposit which can be both immersed or emerged (Leduc, 2013).

2.1.4 Morphological changes

2.1.4.1 Due to sediment loads

The *response* changes of a braiding stream to variations of the sediment inflow are in agreement with the Lane's balance principle. One the one hand, the increase of the sediment entry affects the bed evolution toward an aggradation phase. The experiments of Germanoski and Schumm (1993) showed that the aggradation encourages the development of braiding: the bed relief, surface roughness, banks' number and size increase.

On the other hand, the weakening of the sediment inlet causes the channel narrowing and deepening of the *master channel* in comparison to the smaller low discharge channels. The incising of the main channels causes the flow pattern to change gradually to a single-thread channel (see figure 2.6).

Germanoski and Schumm (1993) flume experiments showed the channel narrowing and incision happens first upstream, the downstream part maintaining its braiding pattern. The narrowing of the channels enhances the erosion upstream and sediment moves downstream. Consequently, the sediment income in the downstream part is higher causing aggradation.

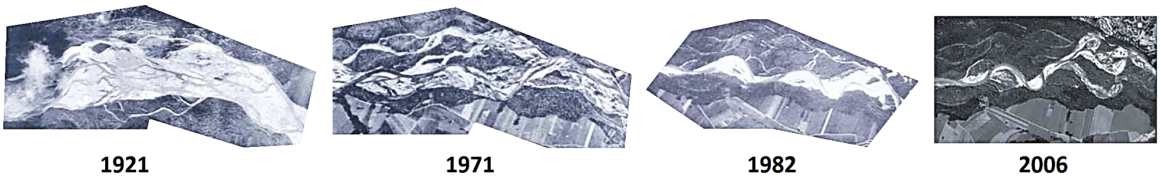

Figure 2.6: The pattern's change of the Isar in Geretsried resulting from the construction of a dam upstream the showed area (Malavoi and Bravard, 2010)

The effect to such forcings will be investigated in detail in the following chapter.

2.1.4.2 Due to valley's topography

As mentioned before (paragraph 2.1.1 page 12), erodible banks are an important parameter for the formation and development of braiding rivers. In this sense, the valley's topography and therefore space made available for water stream to expend will highly influence the resulting channel pattern. The widening of the valley joined to the banks' erodibility will increase the width-to-depth ratio. As a consequence, the carrying capacity will decrease. In this sense, the work of Leopold and Wolman (1957) showed that the braiding doesn't indicate an excessive solid load but an insufficient carrying capacity.

The figure 2.7 shows how, for a same water flow, the valley's topography affects the channel type (see figure 2.7). In addition, the valley's confinement also influences the channels' organization.

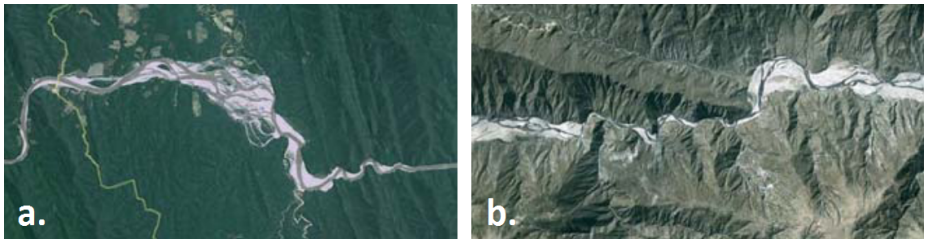

Figure 2.7: Local conversion of the channel type from meandering braiding due to the sudden widening of the valley, b. and from braiding to meandering due to the narrowing of the valley (Andes, Bolivia from Malavoi and Bravard (2010) and Google Earth)

2.1.4.3 Due to the influence of the vegetation

When the system is not supply limited, the braiding pattern is active. Even if the braiding system is in an equilibrium stage, the braiding pattern remains continually in motion. This constant changes of the pattern, and depending on its intensity, inhibits or reduces the vegetation growth. However, the vegetation intensity on braiding beds is both a result of their hydro-morphodynamics and a controlling parameter of the braid dynamics. Indeed, as the results of Tal and Paola (2010) show, the plants also encourage the tendency to of single channels-thread meandering channel by slowing the widening's rate and limiting the channel cutoffs. On another hand, the denser and the more developed is the vegetation cover, the more stable the bar will be.

One can also notice that the pattern's change of the Isar to meandering (figure 2.6) goes along with vegetation growth. The most recent photograph shows a rather established alluvial forest.

2.1.5 Morphometric parameters

In order to characterize a water stream hydro and morpodynamics, several parameters can be studied. However, characterizing braiding streams may require additional care, for the width concept becomes more delicate to handle. Indeed, some other morphometric parameter are better suited to the case of braided systems. The following is a presentation of the parameters which will be used to discuss the results in the next chapter.

2.1.5.1 Bed volume and width averaged slope

The bed volume changes through time give basic information about the considered region of the bed. If the region is subject to aggradation for instance, the volume will increase, and conversely erosion will be reflected by a decrease of the volume. In that sense, if the equilibrium is reached, the sediment volume will become – or oscillate around a – constant. In addition, dividing the studied domain into regions, and analyzing the volume changes of each one, provides interesting information relative to the systems reaction time, "advection", aggradation and erosion processes.

The width averaged slope is also an important indicator of a mophodyanamic systems' behavior. It is calculated by averaging the slope of an width-averaged bed profile.

$$S = \sum_{j=1}^{M-1} \frac{\sum_{i=1}^{N} \frac{Z_{i,j+1} - Z_{i,j}}{N+1}}{(M-1) \times (Y_{i,j+1} - Y_{i,j})} \tag{2.1}$$

in which, S the width averaged slope, i and j are respectively the indices of the point in the X, Y direction , N and M the number of nodes in the X, Y direction and $Z - i, j$ is the node altitude.

Still, a width averaged slope may give biased results since not all the width is mobilized by the water flow. Also, for the case of meandering channel, the averaged inclination overestimates the slope. Therefore, considering the channels' slope individually may be advisable in some cases.

2.1.5.2 Braiding intensity

One can find in literature several parameters to quantify the braiding intensity. A listing of different braiding indices is available in the chapter "The Braiding" of Malavoi and Bravard (2010). For the sake of simplicity, the braiding beds resulting from the numerical model (see Chapter 3) will be discussed in terms of the index of Ashmore (1991): the braiding index is the average number of active channel per transect. The figure 2.8 shows how the active channels are identified in a cross section of a braiding stream model. In this work, a channel is considered as active if the water depth is greater than 2 mm and the width larger than 1 cm.

Yet, this braiding index should be considered with special care. Indeed, it is dependent of the flow rate at the moment of observation. For a same bed, the increase of the flow rate increases the mobilized channel whiting the braiding bed and therefore the active width. The braiding index might increase, but crossing a threshold flow rate, many channels will join in a single channel and the braiding index will start decreasing.

All the models' comparisons conducted in the numerical modeling part relate to models with the same flow rate inflow.

2.1.5.3 Bed Relief Index (BRI)

In order to account of the transversal rippling and variations of the bed's topography, the Bed Relief index was calculated according to Hoey and Sutherland (1991) formulation.

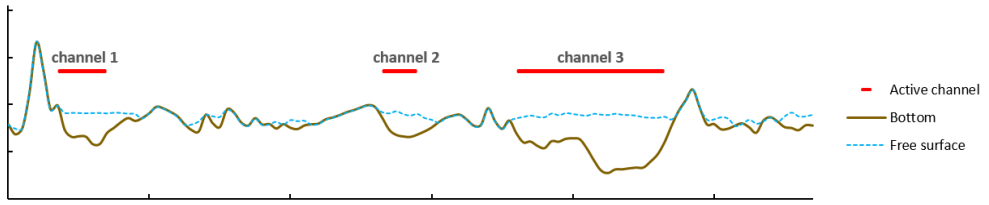

Figure 2.8: Typical transect of a braiding stream model, the red lines represent the channel widths considered as active (not drawn to scale)

$$BRI_{Hoey} = \frac{1}{(X_N - X_1)} \times \sum_{i=1}^{N-1} \sqrt{\frac{Z_i^2 + z_{i+1}^2}{2}} \times (X_{i+1} - X_i) \tag{2.2}$$

The BRI gives an idea about the transversal variation of the bed. A high BRI reflects a transversally varying bed elevation, which can be the sign of incised and/or multiple channels. A low BRI means that the bed topography is uniform along the width.

The advantage is that these results are independent of the flow rate and truly give an assessment of the bed's topography. However, on the one hand, the BRI remains related to the studied bed width, which, in the case of braiding streams is rather subtle. On the other hand, the BRI will fail on capturing the transition from braiding to a meandering like pattern. Indeed, the incision of a single channel in a breading bed will only increase the BRI although the water flows in a single, uniformly shaped, channel.

2.1.5.4 Active BRI

In order to address the issues evoked above, an additional BRI was calculated which only takes account of the active channels (the Active BRI). Indeed, the nodes' altitudes are kept unchanged only if the water depth in the said node is greater than a threshold value. Otherwise, the node's elevation is replaced by the average elevation of the cross section (see figure 2.9).

Figure 2.9: The adjustment of the bed topography, the dry areas are flattered

2.2 Flume experiments

The following is a brief presentation of flume experiments on braiding models, performed during my stay in IRSTEA.

As a reminder, the purpose for which the experiments were conducted is setting of the background relative to braiding systems' dynamics and behavior and thus, planning the numerical modeling work and building a general idea of the expected results.

2.2.1 Material and methods

The flume experiments were performed in the flume of **IRSTEA** in Grenoble. The dimensions of the flume are specified in the figure A.1. The experiment consisted of applying, both solid and liquid, feeding at the inlet of an initially flat sediment bed. Five Runs were performed but only the last two will be discussed hereafter, for the first runs were note very conclusive.

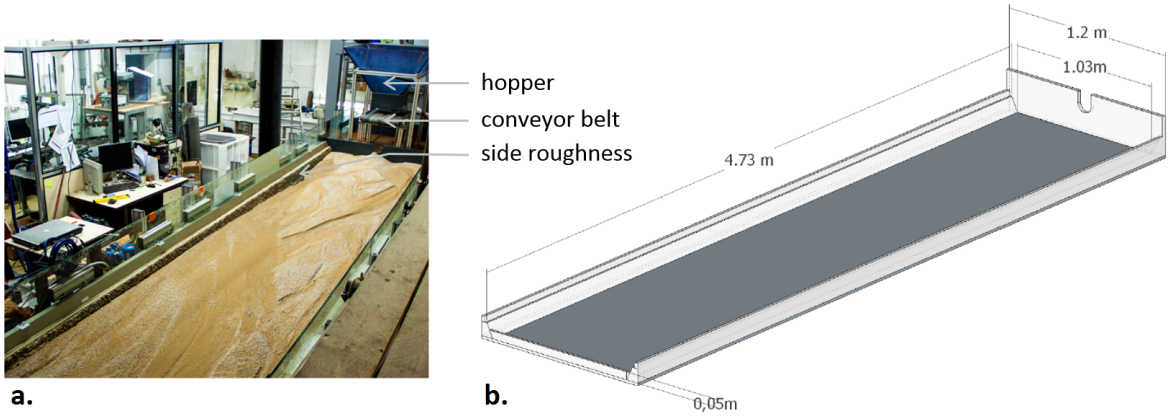

Figure 2.10: Sketch of the flume, the inflow comes from the U shaped hole

In both the Run 4 and Run 5 the slope of the initial bed was 2.7 %. The bed was initially flat with a central incision of 5 cm wide and a depth of 1 cm of a bimodal mixture with a mean sediment diameter of $D_{50} = 1.3\,mm$ (see table 2.1).

Sediment	$D_{16}\ (mm)$	$D_{50}\ (mm)$	$D_{84}\ (mm)$	σ
Fine	0.5	0.7	0.9	1.3
Coarse	1.3	1.5	2	1.2
Mixture	0.7	1.3	1.9	1.6

Table 2.1: Mixture's characteristics, $\sigma = \frac{1}{2}(\frac{D_{84}}{D_{50}} + \frac{D_{50}}{D_{16}})$ is the grading coefficient

In the Run 4 the solid inlet discharge was first 1.59 g/s then was changed to 3.65 g/s after 45 minutes. The flow rate was 0.7 l/s. The whole run lasted 130 minutes. Run 5 lasted 215 minutes with constant sediment feeding rate of 3.65 g/s and a flow rate of 0.6 l/s except for the last 40 minutes. The flow rate was increased at the end in order to observe the effect of a flood on braiding patterns.

2.2.2 Results

Both runs gave quite similar results. Indeed, the resulting braids were, to a certain extent, alike. Also, the experiments didn't last long enough to allow a rigorous analysis of the influences of inflows variations. However, they provided interesting results relative to braiding formation.

Starting from the initial topography, the first morphological changes that one can notice are the deposition of the coarse fraction of sediments as patches along the initial incision. This phenomenon, going along with banks' erosion, agrees with the description of Ashmore (2009) of braiding initiation processes (first mode of the figure 2.3). Therefore, as the sediment deposition increases the bank erosion continues and causes the flow to become shallower, and thus, bars emerge.

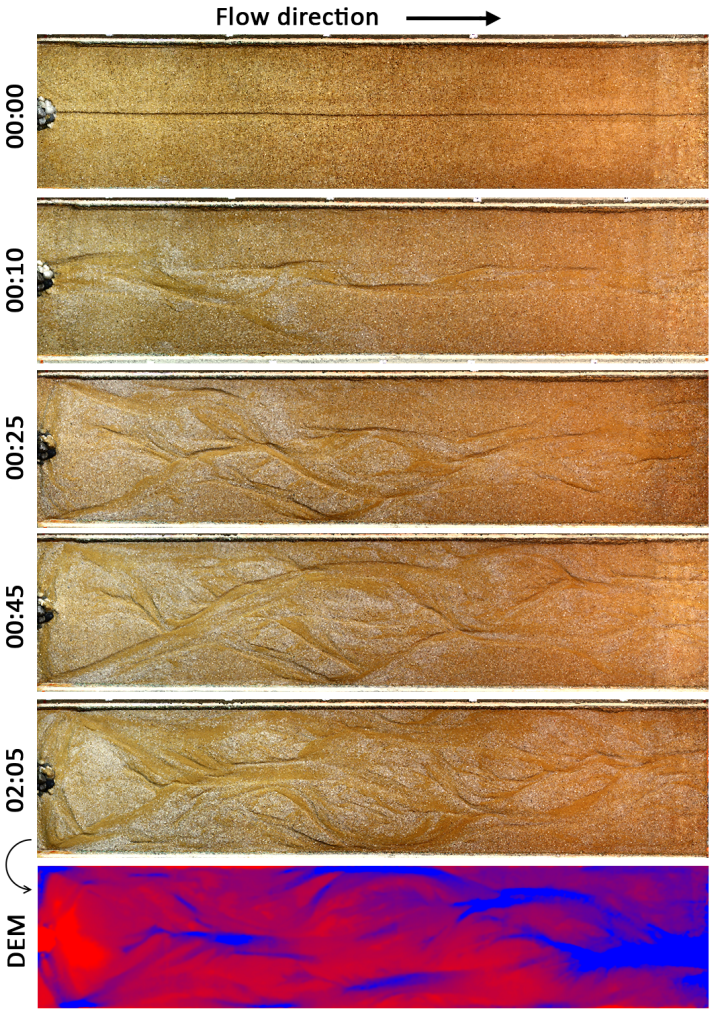

Figure 2.11: Bed evolution in *Run 5*. Due to grain sorting effect, the bars, light colored, are noticeable and the braiding pattern is quite visible. (The partial photographs of the flume were merged using Agisoft Photoscan)

In addition, the general shape of the initial straight incision tends to meander. The bars aren't formed in the exact center of the channel but somewhat alternate (see figure 2.11). This might suggest a crossing mode between the two modes defined in figure 2.3.

Passing this first steps, and as the channel width increases the average water depths decrease and new channels are incised in initial bars. The formation of many avulsion stimulate formation of new channel. This new channels "cut their way" through sediment bed, expand and so on.

This dynamics agreed with the observations of Leduc (2013). Indeed, the sediment used in this flume experiment is the same as the one used in the graded sediment experiments of Leduc (2013). The flow rate, solid discharge and slope were, though, greater in the flume experiment done in this work. This differences impacted both the time and patterns' scales. In fact, the time necessary for the full formation of a braiding pattern,involving the entire flume surface, was approximately 1 hour and 15 minutes, which is a lot less than experiments of Leduc (2013) with graded sediments (the braiding initiation run lasted about 48 hours).

In terms of grains sorting, both experiments' conclusions agreed. The grain sorting effect is highly noticeable in bifurcations, channels merging and areas of flow direction changing. In fact, sediments, depending on their size, don't follow the same path. For instance, at the front of a bar, when flow splits in two channels, the coarse fraction of sediments, due to its higher inertia, fails on following the flow direction, is ditched from the mainstream and therefore deposit on the upper part of the bar (see figure

2.12a) . Also, when two channels meet, the coarser sediments settle whilst the fine ones are transported (see figure 2.12b)

Figure 2.12: Grain sorting in flume experiment, a. the coarse fraction of sediments (light colored) is located at the front of bars, b. the scouring hole turbulences wash away the fine sediments and leaves the coarse sediments

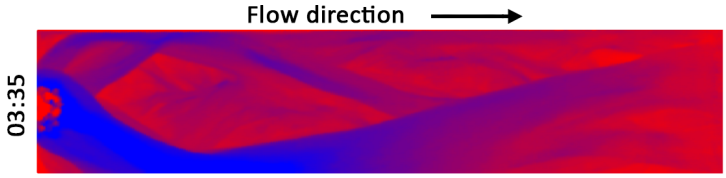

Figure 2.13: Bed elevation at the end of the *Run* 5 after the increase of the inlet flow rate

At the end of *Run 5*, the water flow rate was increased by 150%. The ensuing effect was an almost total revamping of the bed topography. The bed was highly eroded as the sediment transport increased. In addition, the erosion was accentuated at the upstream part of the flume, which tended to reduce the slope. The new channels' shape became wider and almost straight (see figure 2.13) and the resulting bed morphology could no longer be assimilated to a braided pattern. Although it does not accurately reflect the way flood occurrence (the sediment feeding was kept constant), this effect on the bed's morphdynamics rejoined Bertoldi et al. (2010) observations of flood effect on the topography of Tagliamento river.

2.2.3 Purposes and limitations

Flume experiments are a good representation of their real scale prototypes Yalin (1992). They often provide interesting and dense information in hydro-morphodynamics studies, which make them rather interesting for empirical equations' building and also for numerical models' calibration.

The purpose of conducting this experiments was first to consolidate the knowledge regarding braiding rivers morphodynamics, which knowledge will help setting the goals of the ensuing numerical modeling work.

One other perspective of this experiments results was to use the resulting flume's braiding patterns as a starting point for numerical simulation. A quite interesting approach in the sense that it will allow a relatively precise model calibration in addition to a critical discussion of the model's ability to pursue the development of the braiding stream and therefore the highlight of the strength and weaknesses of the model. In that respect, considering relatively small time steps, the evolution tracking will show in what extent the model's behavior is comparable to the physical model's.

The Digital Elevation Model (DEM) of the braiding physical model was acquired by the Photogrammetry method using Agisoft PhotoScan software (see Appendix A page 51). Nevertheless, despite the undeniable advantages of this method, the results were biased. Indeed, in some cases the error in the

bed elevation was of $\pm 0.5\ mm$. Reported to the flume surface, this error will cause an incertitude of $2.4 \cdot 10^{-3}\ m^3$, which is, say, twice the $\pm$ volume changes between two successive measures. Such bias make it impossible to conduct volumetric analysis of the bed's evolution. In addition, the fact that the DEM of the bed was unpredictably distorted, made even the evolution tracking unreliable.

2.3 Conclusion and recommendations

This chapter set the necessary knowledge relative to braiding rivers' pattern, its dynamics and parameters to characterize its morphological evolution. The flume experiments underlined some processes, such as grain sorting, bars formation, avulsion involved in braiding's initiation.

However, this flume experiment's results could only be discussed qualitatively for the data acquisition proved to be, to a certain extent, inaccurate. This drags one's attention to the importance validating the measurement and data acquisition tools in order to have practicable data.

Besides, if the flume experiment are done in order to provide data for a further numerical modeling work, one could use the recommendations listed hereafter:

- Prior investigation of the data necessary to the numerical model calibration;
- Good control and monitoring of the boundary conditions is highly advisable;
- Extra care in measurements and a good quantification of the bias;
- Reduction of the time step between data sets' collection.

Chapter 3

Numerical Experiment

The previous chapter presented a brief description of the processes involved in sediment transport, morphodynamics, braiding and the various modeling alternatives. This chapter will concentrate on the numerical modeling of an example of braiding river.

First, the model setting (from the geometry and boundary condition reasoning to the physical and numerical parameter) will be introduced. Then, the simulations' results will be exposed and analyzed.

3.1 Modeling with TELEMAC-Mascaret system

As previously said, the two dimensional modeling will be performed with TELEMAC-Mascaret system; the hydrodynamic part with TELEMAC-2D and the morphodynamics with SISYPHE. In that sense, a TELEMAC simulation coupled with SISYPHE will require three obligatory files: The geometry, the boundary condition, and the steering file for both TELEMAC and SISYPHE, in addition to a FORTRAN file which gathers the modified TELEMAC and SISYPHE subroutines.

The purpose of these experiments (see chapter 2) was to establish foundation knowledge relative to the braiding phenomena. Accordingly, some of the model's settings and calibration parameters were inspired from, if not the same as, the flume experiment specificities.

3.1.1 The geometry

The domain, the bounded region of the plane which delimitates the mesh, is $10.75m$ long and $1.15m$ wide (see figure 3.8), which is the same width as the flume used in physical modeling and twice its length. In addition, a small rectangle is added umpstream in order to withdrawn the input. This proved to effectively eliminate some stability problems such as massive erosion and/or deposition located at the very first arrow of nodes.

☞ **Remark**: The small rectangular part was set to be non-erodible, otherwise, and in the case when the sediment inflow is lower than the transport capacity of the liquid discharge, the first array of nodes will provide an endless source of sediments. These sediments will directly settle at the entry of the domain (when the width brusquely increases) and cause the model to become unstable.

The used domain can be assimilated to a flat sheet with a central incision of $12cm$ width and $1cm$ depth. A small random vertical perturbation p_i is applied to each node i of the bed, with $max(|p_i|) = 1.5mm$ (see figure 3.8). The slope is taken equal to 3.0% as the bed level decreases going from upstream to downstream.

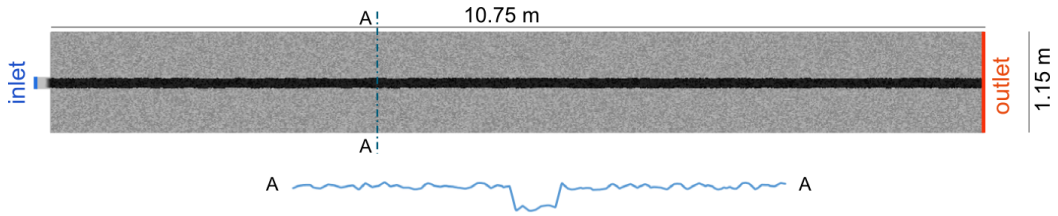

Figure 3.1: The geometry of the model, a. the dimensions of the model reminds the dimensions of a flume, b. detail of the unstructured mesh, c. cross section of the model

3.1.2 The mesh

The meshing has a strong impact on both the geometry and the problem resolution. In fact, the grid quality will determine the accuracy of the idealized model and also the distance (step) between nodes then, consequently, the accuracy of the calculus. However, the finer the mesh gets the longer the computing time becomes. In addition, one should keep in mind the expected accuracy level of the results. Indeed, at some point, an excessive refinement of the mesh will only increase CPU time with no significant improvement of the results.

Besides, in this work, the same mesh will be used for both the hydrodynamics and morphodynamics. Accordingly, the choice of the mesh level of refinement is very crucial and will have, inevitably, a considerable impact on the results.

The meshing should be refined enough (small distance between two successive nodes) in order to represent well the braiding morphology. On the one hand, a "coarse" grid will either not allow the incision of small channels or will result the formation of shallow ones. This can be problematic insofar as, for a given stream power, a channel with a small width and a great depth induces more bedload transport (Ashmore, 1988). On the other hand, the hydrodynamic of narrow channel is poorly modeled with coarse meshes.

Both the shallow water equation (TELEMAC-2D) and the Exner equation (SISYPHE) with, respectively, finite element method and finite volume method, are solved using a computation mesh of triangular elements. This two methods are defined on meshes of data points. In such mesh, every node has a fixed number of predefined neighbors. Therefore, the connectivity between these neighbors is used to define mathematical operators such as the derivatives. In our case, these operators are then used to construct the equation to simulate.

The final mesh was chosen to be an unstructured grid of triangular elements with a default edge length of 0.015 m and a maximal edge growth ratio of 1.1. The resulting node and edges count is presented in table 3.1.

Nodes	**61212**
Elements	**120485**
Default egde lenght	**1.5 cm**
Boundary nodes	1937
Inlet nodes	9
Outlet nodes	93

Table 3.1: Count of the domain's nodes and edges

☞ **Remark**: The refinement of the 2-D mesh is highly recommended in regions of high interest, near the banks and slope break for instance. However, since the purpose of this work is to analyze the ability of TELEMAC2D/SISYPHE model to reproduce the initiation and evolution of the braiding pattern, the

initial topography was chosen to be flat with a central incision. Therefore, the mesh (or the nodes spacing) was chosen to be as uniform as possible throughout domain. Any localized mesh refinement will inevitably influence, even slightly, the hydrodynamics and subsequently the morphodynamics.

3.1.3 Modeling organization

Before presenting the boundary conditions (section below), it is suitable to first present how the following modeling work is organized.

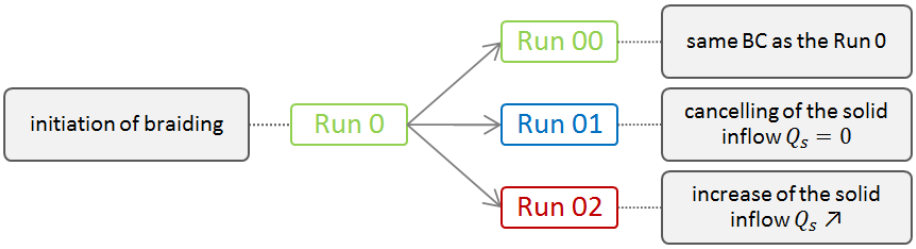

Figure 3.2: Simulation organisation

Figure 3.2 summarizes runs' organization. First, *Run 0* starts from the initial model presented before, *Run 0* is therefore the braiding formation model. Second, and once the braiding is established, three major runs follow. Basically, *Run 00* is the continuity of *Run 0*. The boundary condition are kept the same as prior *Run 0*. The two other runs, *Run 01* and *Run 02*, are respectively, erosion and aggradation. In the first one, the sediment inflow was stopped, and in the second one, the sediment inflow was increased.

3.1.4 Initial conditions

The initial state from which the simulation starts is a flat sloping bed (3%) with a central incision of 10 cm and a constant water depth of 2 mm on the whole domain. This last condition didn't affect the behavior of the model and was chosen only in order to insure the stability of the first time step's.

3.1.5 Boundary conditions

The boundary conditions (BC) are kept as simple as possible with a constant discharge and sediment inflow at the inlet. At the outlet boundary, the free surface level is taken constant and the solid transport rate is calculated with the specified transport formula.

Runs	**Inlet**		**Outlet**	
	$Q_s\ (m^3/s)$	$Q_l\ (m^3/s)$	$Q_s\ (m^3/s)$	$Z_{freesurface}\ (m)$
Run 0	7.46×10^{-7}	3.75×10^{-4}	Calculated with sediment transport formula	$Constant$, 2 mm above the initial bed level
Run 00				
Run 01	0			
Run 02	1.15×10^{-6}			

Table 3.2: Boundary conditions for each run

The table 3.2 gives the different boundary settings for each one of the runs. As one can notice, and in agreement with the previous section, the purpose of *Run 00* is to see the braiding behavior in the same

conditions in which it was established. In *Run 01* the sediment inflow was increased by 54 % and was completely stopped for the *Run 02*.

3.1.6 Modeling parameters

Unless otherwise specified, the modeling parameters which will be presented hereafter will remain the same for all the runs. It is crucial for conducting an isolated analysis of the model response to different forcings.

3.1.6.1 Numerical parameters

The 2-D simulations were performed using the finite element method for the hydrodynamics and the finite volume method for the morphodynamics. The scheme used for the advection of velocities and water depths were, respectively, the method of characteristics scheme and the mass-conservative distributive PSI scheme. This parameters agree with the default numerical parameter of TELEMAC.

The used solver for the hydrodynamic propagation step is the conjugate gradient on normal equation method and conjugate gradient method for the turbulence model.

Regarding the tidal flats areas, TELEMAC-2D first detect the tidal flats zone, the equations are solved everywhere, and then a correction of the free surface gradient is applied.

Considering all these numerical parameters, and in agreement with the specified boundary conditions, the optimum time step of each iteration was therefore $t = 0.01s$. Which gives 3600 / 0.01 = 360000 iterations for 1 hour simulation.

3.1.6.2 Hydrodynamics

The boundary conditions are already presented in previous sections. The remaining hydrodynamics parameters to be presented are therefore the turbulence model and the bottom friction law.

The turbulence model considered is the "constant viscosity" model, the advantage of this model is that it requires a lower refinement level of the mesh (compared to the K-epsilon) and therefore reduces the CPU time. The overall viscosity coefficient (molecular + turbulent) is $10^{-6}\ m^2/s$ (water at $25°C$). This velocity diffusivity parameter has an impact on both the shape and extent of recirculation.

Bottom friction law, it is one of the most important hydrodynamics parameters, for it conditions the water velocity and also the bed shear stress, which controls the sediment transport rate. The friction law is considered to be the same in the whole computation domain. The used friction law is the Strickler's law with the a Strickler coefficient of $K = 50m^{1/3}/s$.

One should note that the Manning-Strickler is not well suited for small relative flow depths (Ferguson, 2010; Rickenmann and Recking, 2011).

3.1.6.3 Morphodynamics

The simulation parameters for the morphodynamic module (or the SISYPHE steering file's inputs) are as follows.

Sediment mean diameter Unless specified otherwise, the sediment used has a mean diameter of $D_{50} = 0.8\ mm$. Which corresponds to coarse sands (according to the Wenthwort grain size chart). The use of uniform particle size allows to conduct an analysis without consideration of the hiding and exposure effects.

The transport formulas which was used for the four runs (0, 00, 01 and 02) is the classical Meyer-Peter-Müller formula (see 1.2.3 page 3). In addition, the Ashmore (1988) and Van Rijn (1984) formulas was used in other following runs.

Shields parameter The critical Shields number is taken equal to $\theta_c = 0.047$ when Meyer-Peter-Müller formula or Van Rijn (1984) formula are used. However, when the simulation was run with Ashmore formula (1988) the critical Shields parameter was set to $\theta_c = 0.045$ (see section 1.2.3).

Bed slope effect and deviation On the one hand, the modeling includes the effect of the (transverse) slope on sediment transport. It amounts of taking in consideration the direct effect of gravity on particle on a sloping bed. Indeed, the gravity adds a force's component which can encourage or discourage the initiation of the transport, in other terms; the slope effect has an influence on the threshold shear-stress (Soulsby, 1997). The critical Shields θ_c parameter is therefore adjusted via the Soulsby (1997) formula. Depending on the slope angle, the angle of repose and the relative direction of the flow to the slope direction, the threshold shear-stress value will either increase or decrease. The new critical Shields $\theta_{\beta c}$ parameter is calculated according to Soulsby (1997) formula (3.1) (see figure 3.3).

$$\frac{\theta_{\beta c}}{\theta_c} = \frac{\cos\psi \times \sin\beta + (\cos^2\beta \times \tan^2\phi_i - \sin^2\psi \times \sin^2\beta)^{1/2}}{\tan\phi_i} \tag{3.1}$$

On the other hand, the change of the direction of solid transport is also accounted for by the use of deviation's formula (Tassi and Villaret, 2014; Talmon et al., 1995):

$$\tan\alpha = \tan\delta - T\frac{\partial Z_f}{\partial n} \tag{3.2}$$

Where α is the direction of solid transport, δ is the direction of the bottom stress in relation to flow direction, Z_f is the bed level and n the coordinate along the axis perpendicular to the flow. T is calculated according to Talmon et al. (1995) formula:

$$T = \frac{1}{\beta_2\sqrt{\theta}} \tag{3.3}$$

in which β_2 an empirical coefficient taken equal to 0.85 (which is suitable for flume experiments).

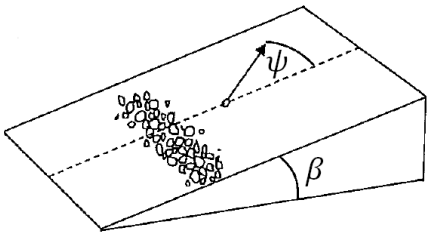

Figure 3.3: Motion of sediment on a sloping bed. Where ψ is the flow angle and β the slope angle (Soulsby, 1997)

In addition, De Linares (2007) recommends the use of the bed slope effect and deviation parameter joined. The account of only the bed slope effect may lead to the establishment of unrealistic and steep slopes. Indeed, the slope effect increases the sediment transport rate in sloped areas. However, this effect will "soften" the bedform only if the sediments are deviated in the descending slope direction.

Secondary currents Although the model is two dimensional, SISYPHE allows to take into account influence of the secondary currents, such as helical or spiral flow effect, on sediment transport. Indeed, the bedload transported sediments are deviated from the main stream because of such effects (Tassi and Villaret, 2014; Wu, 2008). The sensitivity analysis conducted by Schuurman et al. (2013) on his numerical model of braiding rivers highlighted the importance the consideration of these effects. Neglecting the secondary currents influence slowed the establishment of braiding and resulting bars and channels were shallower. The deviation angle δ caused secondary currents effect is implemented in the model via Engelund (1974) formula:

$$tan\delta = 7\frac{h}{r} \tag{3.4}$$

in which

$$r = -\rho\alpha\frac{U^2}{g\frac{\partial Z_s{}'}{\partial y}} \tag{3.5}$$

The coefficient α is taken equal to 1, in agreement with the recommendation to relatively smooth beds.

☞ **Remark**: The Appendix B page 55 presents the steering files for the TELEMAC2D and SISYPHE relative to the simulation of the $Run\ 0$.

3.2 Results presentations' plan and expected results

The following sections are the presentation of the results achieved with the 2-D modeling. First, the Run 0 and Run 00 results will be exposed in the same section. The second section will present the results of the Run 01 and the third the results of Run 02. Also, additional simulation models will be presented.

According to flume experiments' observations (see chapter 2) and literature revue, the model is expected to start with bar formation processes, and then to initiate the braiding pattern. Therefore, on the one hand, once the braiding pattern is established, the increase of the sediment supply should lead to an aggradation phase in which the braiding should continue developing. On the other hand, the cancellation of the solid inflow will lead to a progressive narrowing of a main channel and so the tendency to a meandering pattern.

3.3 Results

3.3.1 Establishment of the braiding pattern(*Run 0 and Run 00*)

As a reminder, the bed's slope is 3%, the solid inflow is $7.46 \times 10^{-7}\ m^3/s$, the liquid inflow is $3.75 \times 10^{-4}\ m^3/s$ and the transport formula used is Meyer-Peter-Müller (1948).

3.3.1.1 Emergence of the braids

First, as the simulations starts, one can notice the changes on the central incision. Indeed, the banks are eroded and therefore the central incision's width increases. The sediments coming from the inlet boundary added to the mobilized volume from the bank erosion contribute to the increase of the bed level. This, added to widening of the channel, increases the width-to-depth ratio (see figure 3.4). In other terms, the channel becomes shallow and therefore the sediment transport capacity decreases. The sediment are deposed and the first bars appear.

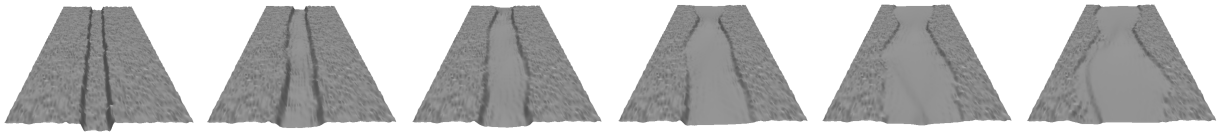

Figure 3.4: Bed evolution through time (*Run 0*)

The bar develop a curved convex shape with a central "peak" (see figure 3.5). This causes the water flow to split and flow on the sides of the central bar. Passing the central bar, the junction of the two channel streams (confluence) lead the increase of the transport capacity and the appearance of a pool. One can also notice the forward migration of this bars in the downstream direction.

This pool formation and migration processes are well described in literature (Leduc, 2013; Ashmore and Parker, 1983). The confluence of channels creates a highly turbulent zone which destabilize locally the bed and lead to the digging of a scour hole. The migration of the channels and therefore their junction cause then also the migration of this scour hole.

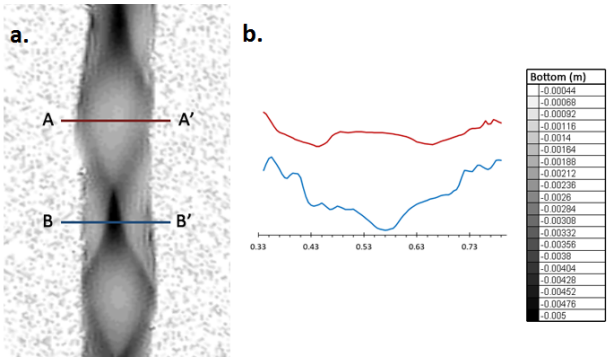

Figure 3.5: The formation of bars, a. the bed's topography (*Run 0*), b. cross section of the bed, in red the cross section of a bar and in blue the cross section of a scour hole

One can also notice that the velocity field is not always symmetrical. Indeed, the velocity vectors tend to oscillate (see figure 3.6).

This first phase lasted about 40 minutes. At a certain point, the bars are exposed and the continuous aggradation causes the elevation of the bed level. Consequently, some channels start flooding and the water start flowing on what can be assimilated to a "flood plain". Therefore, if the shear stress is high enough, the incision of a new channel initiates (see Appendix C). These observations suggest that the braiding initiates by combined aggradation and erosion processes.

The forward migration of this bars toward the downstream direction is also observable on the model (Appendix C page 59).

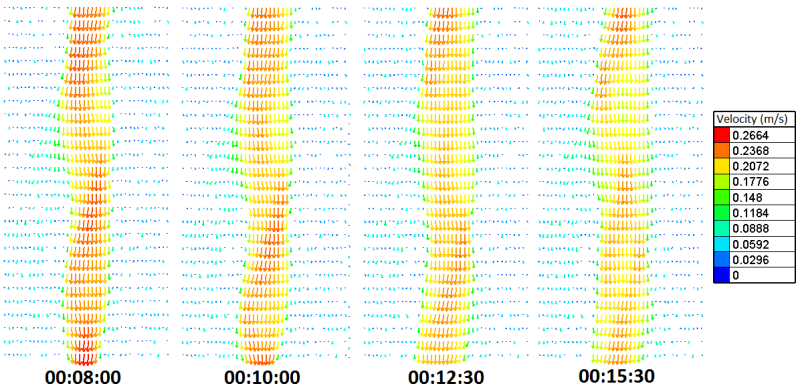

Figure 3.6: Velocity field (*Run0*)

3.3.1.2 Braiding

After 1 hour, the bed morphology becomes similar to the braiding patterns observed in both in the field and flume experiments. The braiding morphology is rather realistic and the model shows several noteworthy morphologies typical to braiding rivers. After the first hour to the end of *Run 0*, the braiding develops but in a much slower motion than for it initiation. Figure 3.7 shows the resulting bed topography after 2 hours and 13 minutes (the end of Run 0). One can notice the splitting/meeting of multiple channels, the bars and the scouring holes.

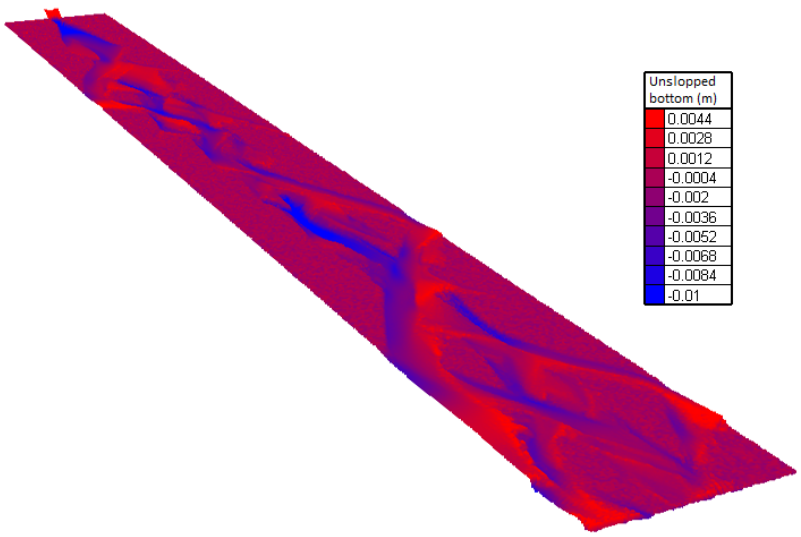

Figure 3.7: Resulting bed topography at the end of *Run 0* (02:13:00)

Passing the second hour to the end of *Run 00*, the bed seems to evolve and change. However, analyzing water depth, water velocities and solid discharge reveals that even if the bed relief seems undulating and varying, the water mostly flows in single channel. Consequently, one can state that the highly rippled bed forms are only the remainings of a previously braiding stream. This issue will be discussed in more details in the next section.

3.3.1.3 Analysis of the results

This subsection will be dedicated to the analysis of the results obtained from *Runs* 0 and 00. The discussion will be based on some morphometric parameters introduced in chapter 2.

Data extraction grid The bed levels and water depth necessary to calculate the morphometric parameter were extracted from the model in specific points. The whole of these points can be assimilated to the node of a structured grid. Indeed, the spacing of these nodes is constant in the x and y direction: $\Delta x = 0.01m$ and $\Delta y = 0.075m$.

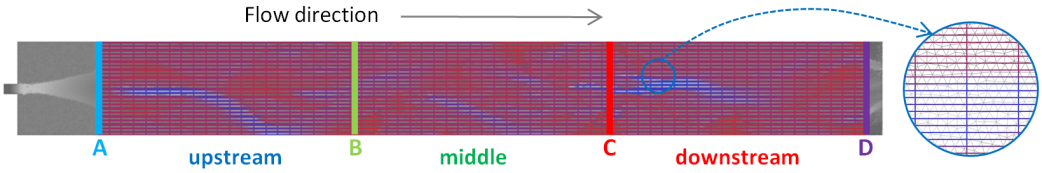

Figure 3.8: Data extraction zone with a structured grid

The use of a uniformly spaced data extraction grid is convenient, for it eases the data operating and also facilitate the calculation of indices which require, for instance, elevation information along a transect (such as the BRI and the braiding index). In addition, the data extraction grid doesn't cover the entire computation domain (see figure 3.8). The reasons near the boundaries are avoided.

Data extraction transects For each run, the bedload discharge changes through time were extracted in four cross sections. Their locations and names are specified in the figure 3.8. Thus, these four sections delimitate three zones which will be designated by upstream zone, middle zone and downstream zone.

BRI and active-BRI As a reminder, the Bed Relief Index of Hoey and Sutherland (1991) (BRI) reflects the transversal variability of the bed around the average elevation and the active-BRI is the BRI with only the account of active channels (in here the threshold value over which a channel is considered as active is a water depths of d$h = 2\ mm$). Both are expressed in meters.

The figure 3.9 shows the BRI and active-BRI evolution over time for *Run 0-00*. The active-BRI is lower than the standard BRI because, at the beginning, not all the flow is contained in the first incision, and therefore a thin layer (lower than 2 mm) of water pours over the banks. During the first 30 min both the indices decrease, which is due to the shallowing of the central incision. This first profile smoothing phase is followed by a renewal of the transversal irregularities of the bed which indicates bar formation.

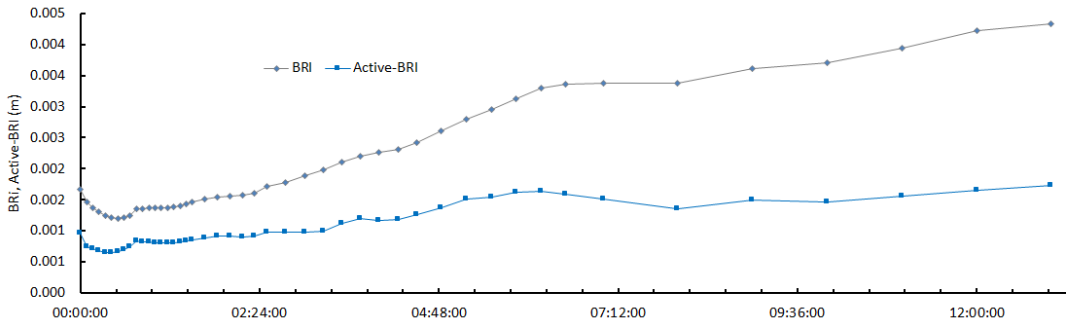

Figure 3.9: Evolution of the BRI and active-BRI of $Run\ 0-00$

The bars emergence is also captured by the active-BRI. Indeed, a small decrease can be noticed around the first hour, whilst the standard BRI increases. This means that the bed continued changing its transversal profile while a dry zone has emerged.

The continuous increase of the BRI means that the bed is constantly remodeled. However, passing the sixth hour, the BRI's evolution slows and the active-BRI becomes almost constant. This ascertainment

reflects a tendency of the system to convert to a single-thread channel: the water flow migration to a single channel phase is shown by the decay of the Active-BRI and a slight increase of the standard BRI. Then, the single channel start incising, which increases the total horizontal variation of the bed but leaves the active active-BRI almost constant.

It is indeed interesting to plot both these indices. As both consider the same width, the growing divergence between the BRI and active-BRI proves that even though the bed is remodeled, only a small fraction conveys the water.

Slope Three average slope are calculated, the slope of the upstream half of the data extraction zone (see figure 3.8), the slope of the downstream half and the mean slope.

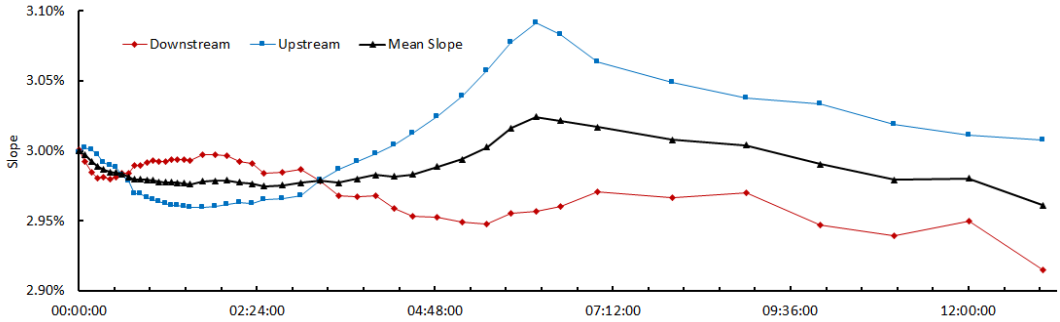

Figure 3.10: Evolution of the slopes of $Run\ 0-00$

First thing noticeable, is that $Run\ 0-00$ was characterized by three phases. The general shape of the bed started by becoming convex, then, after the 35 minutes, became concave, and once again became convex. The first phase was due to the deposition of inlet sediments at the upstream part of the flume on account of the sudden widening of the domain. Consequently, the sediment deficit caused the erosion of the middle of flume, which sediment will be deposit in the downstream part. This observations rejoin the observation of Leopold and Wolman (1957) showed in figure 3.11. This schematic profile clearly shows that the upstream half has a higher mean slope value. In addition, the profile shape seemed to translate in the downstream direction, the aggraded pile shifting will gradually reverse the convexity (passing from convex to concave), and again, when the "sediment wave" reaches the downstream part, the bed shape regains its convex like shape. This processes is clearly seen in the figure 3.10. Indeed, the conveying of the sediment wave affects the partial mean slopes.

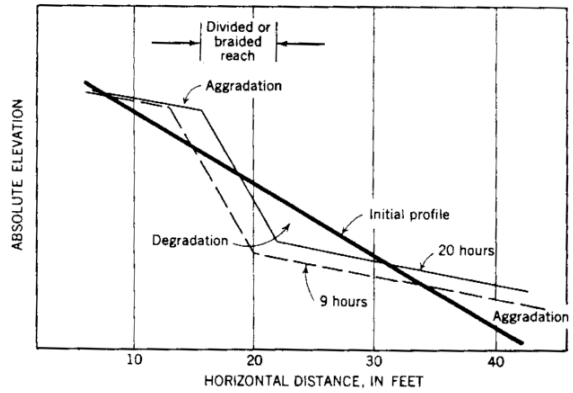

Figure 3.11: Diagrammatic profiles of the bed's evolution (Leopold and Wolman, 1957)

However, slope decreasing indicates an adjustment of the topography in order to adapt to the boundary condition (or control variable). This can indicate that the system is at sediment supply limitation.

Nevertheless, at a certain point a width averaged slope accounting for the total width became somewhat irrelevant. In fact, the BRI and visual analysis of the bed topography showed that after the sixth hour the stream transform to a single-thread channel. Consequently, only the topography of a small fraction of the width reflects the hydro-morphodynamical status of the system. Calculating the slope along the main channel showed agreement with this statement, for the slope of the main channel at the end of Run 00 was 2.59%, which is less than the mean slope of the whole data extraction zone.

Volume Figure 3.8 shows the the domain's fragmentation to the three subdomains considered too hereafter. The volume is supposed to be 0 at the beginning.

As figure 3.12 shows, the system is continually aggrading.The volume evolution of the three parts considered separately shows how bed changes occur and how the slope changes occur. Also, the decrease of total volume between the sixth and seventh hour of the Run 0 can be correlated to the beginning of the abandonment of the braiding pattern to a single channel morphology.

Other interesting remark is the rapid increase of the volume of the downstream part after the ninth hour. One can notice that the downstream aggrade (and the width averaged slope decreases see figure 3.10), but the middle part volume remains practically constant. Therefore, the central part of the flume only conveys the sediments from the upstream to downstream in a rather stable way, which is more akin to the behavior of single-thread channels.

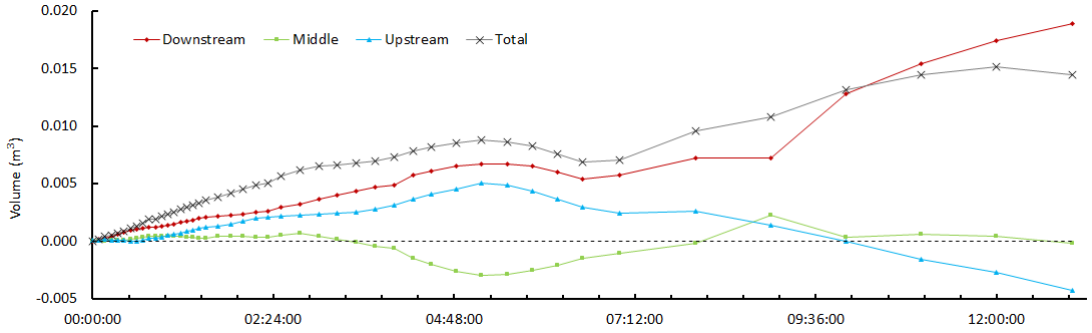

Figure 3.12: Evolution of the bed's volumes of Run 0 – 00

Bedload transport rate The sediment transport is monitored at 4 transects (see figure 3.8) which delimitate the surfaces considered in the volume analysis. The location of the transects eases the confrontation with volume changes. Although, the sediment transport rate gives basically the same information as the volume formation, the bedload transport rate brings more insight on the inertia of the sediment transport (see figure 3.13). Indeed, one can notice for instance the high variability of sediment transport and its relative stabilization after the ninth hour (except for the last transect in which the transport rate remains highly varying; which can also be related to the fact that the D section is close to the outlet boundary).

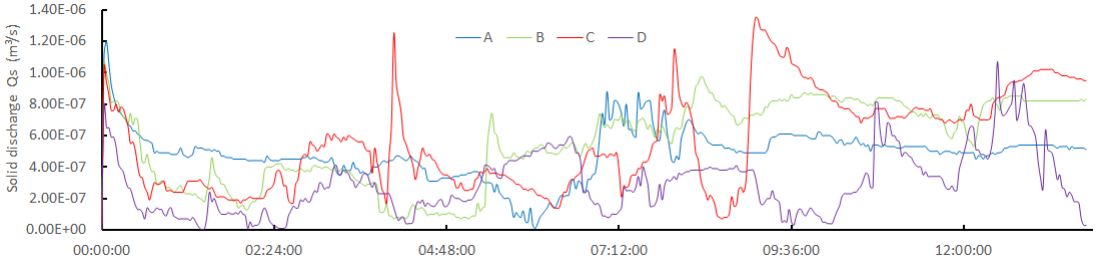

Figure 3.13: Evolution of bedload rates at different transects in Run 0 – 00

In addition, the simulation results showed that despite the multitude of channels, only a few (one to two in this model) are responsible for the solid transport and bed's morphological changes (see figure 3.14). This agrees with the observations of Ashmore et al. (2011).

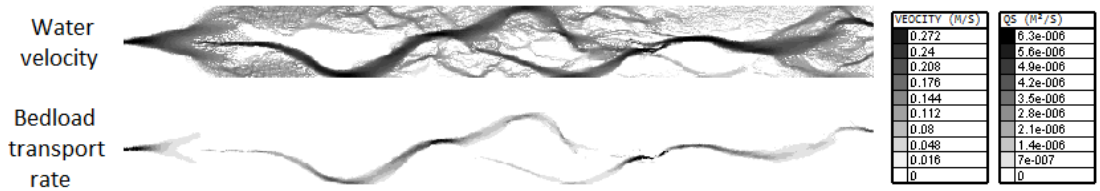

Figure 3.14: Water's velocity field vs. bedload transport rate. The channel's activity is limited to a narrow band along one to two channels.

3.3.2 Erosion (*Run 01*)

This section investigates the response of a braided model (resulting from RUN 0) to the cancelling of sediment feeding. The flow rate was kept constant and the sediment inlet was stopped.

☞ **Remark**: As a reminder, the following runs (erosion and aggradation) start from the final stage of the Run 0. The new boundary conditions of each of the next runs occur after 02 : 15.

BRI and active-BRI The Bed Relief Index increases as the bed evolves in time (see figure 3.15). The results exposed in Appendix C show indeed the incision of channel due to the sediment deficit. The incision of a main channel adds to previous bed variation, and therefore the BRI continues on increasing. However, the active-BRI only accounts of the variations of bed surfaces under water (the threshold value is taken equal 2 mm). In fact, one can notice the relatively slow evolution of the active-BRI, which is a reflect of two phenomena: the narrowing of the main channel with the decrease of its width-to-depth ratio and the progressive conversion to a single-thread channel, then its ongoing narrowing, which happen from the upstream to the downstream (see Appendix C).

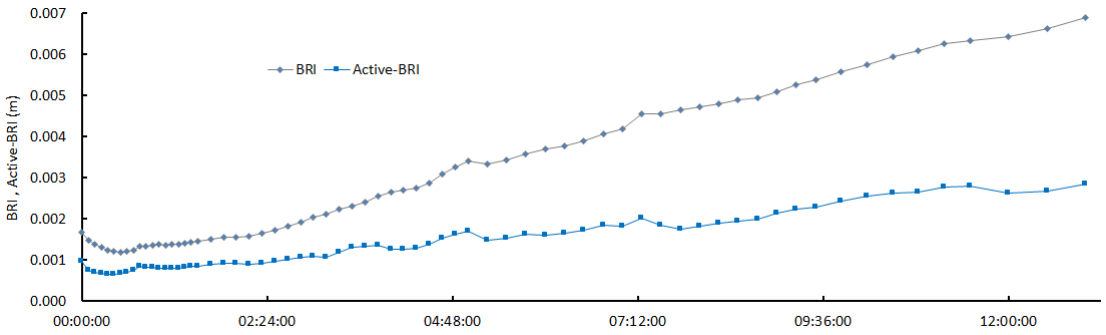

Figure 3.15: Evolution of the BRI and active-BRI (Run 01 starts at 02 : 15)

In comparison to the values of Run 0 – 00, which were also increasing. One can notice that the Run 01's values of BRI and active-BRI are higher, which reveals that the single channel resulting from Run 01 is narrower.

Here again, the increasing divergence of the two indices reflects the change of the alluvial style of the model, which was rather expectable, since the sediment supply was stopped.

Slope The mean slope of the whole bed continuously reduces along the simulation (see figure 3.16). This result agrees with general field and flume observations and also with the Lane's Balance principle. However, the upstream and downstream mean slope considered apart, show how the slope adjustment process occurred. Indeed, the upstream slope remained lower than the downstream one for about 9 hours. The width average bed profile had a concave shape during this phase. This observations are the result of the transfer of the sediment budget from upstream to downstream, which describes the slope adjustment process. After this adjustment period, the bed slope seemed to stabilize.

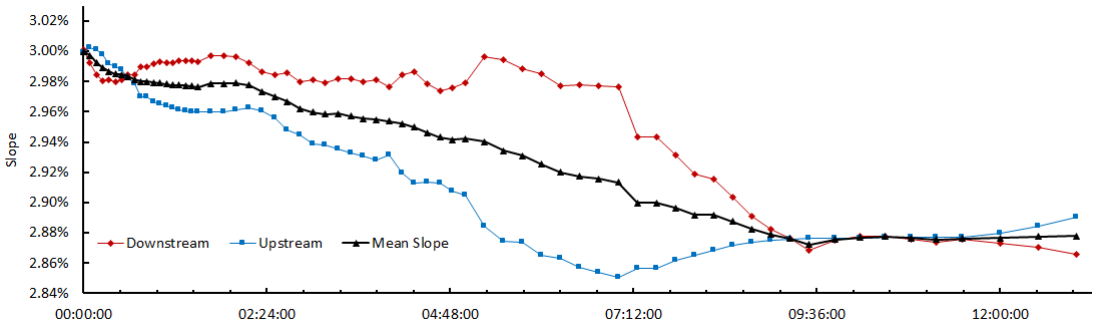

Figure 3.16: Evolution of the slopes (Run 01 starts at 02 : 15)

Considering the transformation of bed style to a single channel one. The slope of a width averaged profile becomes quite irrelevant. In that sense, the slope of the main channel was measured. The channel slope was equal to 1.99%, which is less than the mean slope of the whole bed.

Volume and bedload transport rate As soon as the sediment inflow is stopped, the bed's volumes start declining 3.17. The observations made in the slope analysis part are verified. The upstream was eroded, the sediments passed by the middle part, and then caused aggradation of the downstream part.

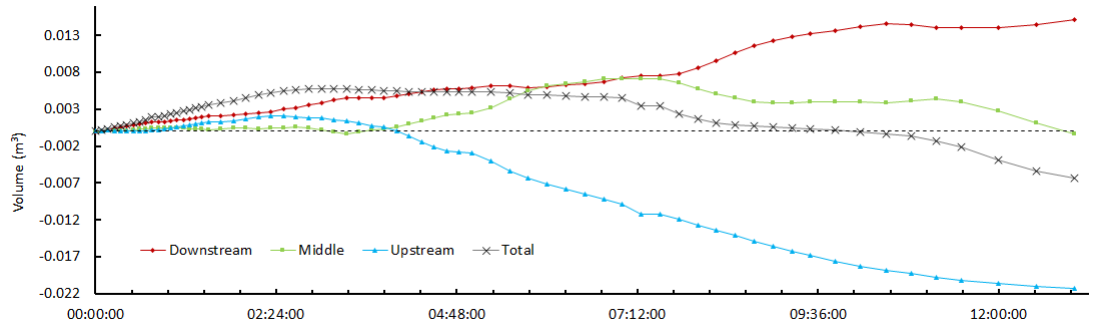

Figure 3.17: Evolution of the bed's volumes (Run 01 starts at 02 : 15)

Sediment transport also confirms this observations (see figure 3.18) and shows a general decrease of the sediment dynamics at the end of Run 01. Actually, the graph represents the transport capacity of each transect. The transport capacity is equal to the sediment transport rate only if all the sediments can be mobilized. At the section A the water start flowing on the non-erodible font, which biased the result (the dotted part of the plot).

According to this results, one can state that the model succeeded on reproducing the effect of the weakening (or canceling) of the sediment inflow. A single channel starts developing, incising and narrowing. Consequently, the slope adjust in order to bring the stream to the equilibrium state relative to the new boundary conditions.

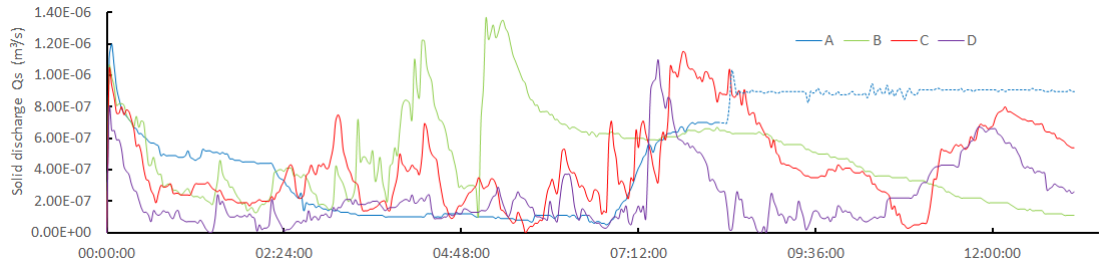

Figure 3.18: Evolution of the bedload rates at different transects (Run 01 starts at 02 : 15)

3.3.3 Aggradation (*Run 02*)

This section investigates the response to braiding model (resulting from Run 0) to the increase of the sediment feeding. The flow rate was kept constant and the sediment feeding was increased by 54%.

BRI and active-BRI The Hoey's BRI continues increasing, as in the two previous runs. The bed changes in appendix C shows indeed an incision of a main channel. In fact, the sediment feeding didn't maintain the braiding morphology.

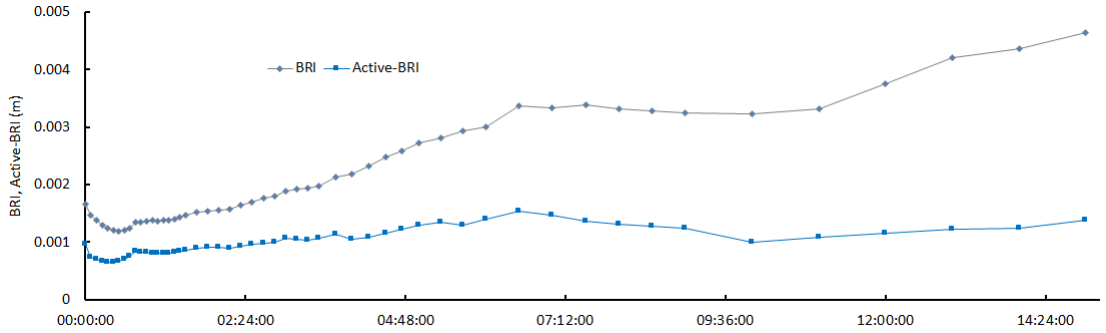

Figure 3.19: Evolution of the BRI and active-BRI (Run 02 starts at 02 : 15)

The active-BRI shows that a certain equilibrium is reached after the seventh hour. The active-BRI remained almost constant, meaning that the dominant channel didn't incise nor flatten. However the increase of the standard BRI combined with a constancy of the active-BRI indicated that the total bed's topography encountered some changes, but the average channel's shape remained at rest. In other terms, although it moves within the domain, the dominant channel's shape remains almost constant.

Slope The slopes variations (see figure 3.20) remind the ones of Run 0 – 00. The profile's convexity changes compare well. A closer look to this slope variation showed that the shifting from the concave profile to a convex one happens sooner in this run than in Run 0 – 00. The aggradation process at the upstream part is accelerated by the abundant sediment feeding.

The peak of the total and upstream slope at 06 : 30 is characteristic of the collapse of the sediment deposit at the inlet and its gradual propagation through the domain.

Volume and bedload transport rate The volume and bedload transport rate increases are noticeable in the figure 3.21 and 3.22 respectively. The system's volume increases gradually until a certain thresh-

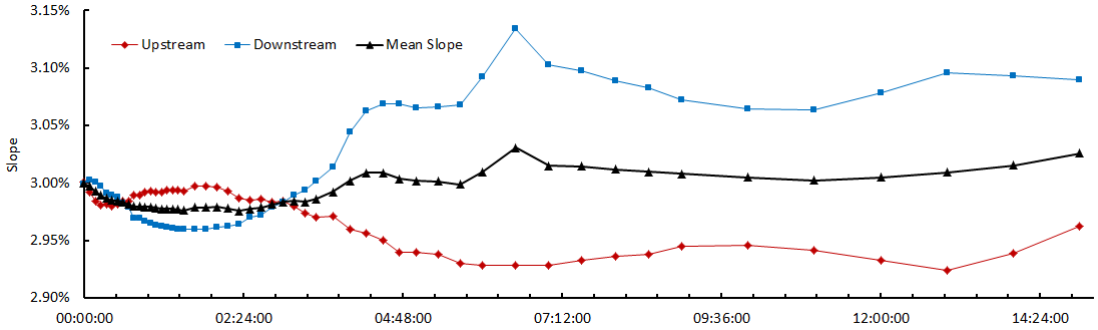

Figure 3.20: Evolution of the slopes (Run 02 starts at 02 : 15)

old value is attained and then decreases. This diminution is due to the discharge of the sediments caused by the failure of the heap of sediments previously formed.

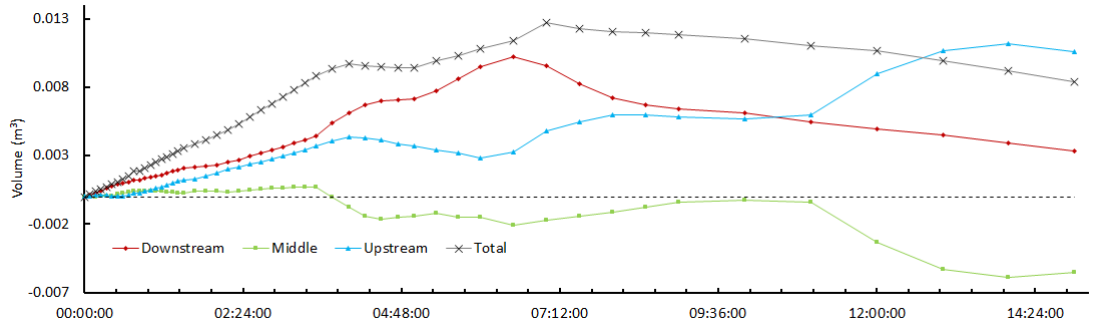

Figure 3.21: Evolution of the volumes (Run 02 starts at 02 : 15)

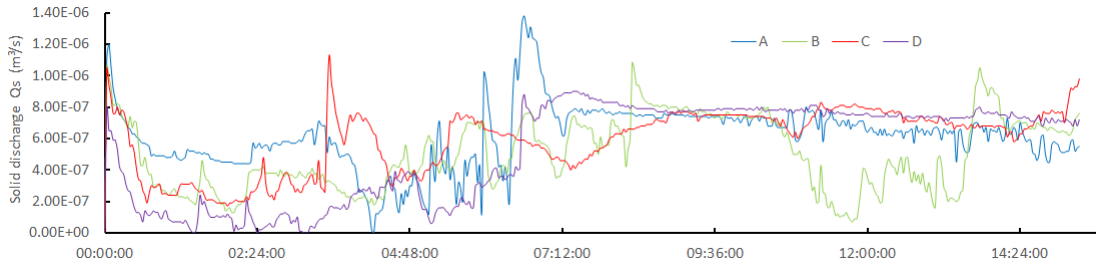

Figure 3.22: Evolution of the bedload rates at different transects (Run 02 starts at 02 : 15)

The transport rates seem to stabilize, which agrees with the hypothesis of the systems achievement of equilibrium. Tough, the transport rate at the transect B remains variable, which is a result of the fact that the transect B cuts the bed in a multiple active channels section (see appendix C), the transport dynamics are therefore fluctuating.

3.4 Additional results

The following is a short presentation of other braiding streams simulations. Their aim was to broaden the view of TELEMAC2D/SISYPHE abilities on reproducing braiding morphologies with the account of other parameters. Besides, the analysis of these new results will provide additional bases necessary to the assessment of the models strength and weaknesses.

Hereafter, the models' results will be discussed briefly and mostly in a qualitative way.

3.4.1 Variation of the water inflow

Two additional model runs were done in order to investigate the influence of the variation of the water discharge on the maintaining of the braiding pattern. The first one accounted for the flow rate variation using a hydrograph with a randomly oscillating discharge over time. In the second one, the direction of the flow at the inlet was changed over time in a random motion.

On the one hand, the variation of the flow rate wasn't very conclusive. The hydrograph random variation didn't prevent the progressive transformation of the pattern to a single-thread channel.

On the other hand, the random variation of the velocity vectors direction gave rather interesting results. The braiding pattern seemed more developed (see figure 3.23) and "maintained" longer than in the case of constant inflow direction.

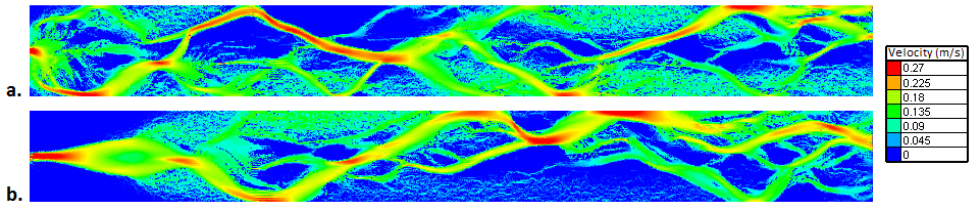

Figure 3.23: Water velocity field of the after 3 hours, a. with random variation of the inflow velocity vectors, b. with a a constant direction of the inlet's water velocity vectors

3.4.2 Ashmore and Van Rijn

Both these bedload transport formulas are presented in the chapter 1 section 1.2.3. The Van Rijn formula was already available in SISYPHE's subroutines and the (Ashmore, 1988) formula was implemented in the model.

The results produced by each one of these formulas were quite different (see figure 3.24). The beds topography seems more evolved for the Van Rijn model. Compared to the results of the previous runs, one can state that the Ashmore formula underestimates the sediment transport comparing to Meyer-Peter-Müller and Van Rijn formulas.

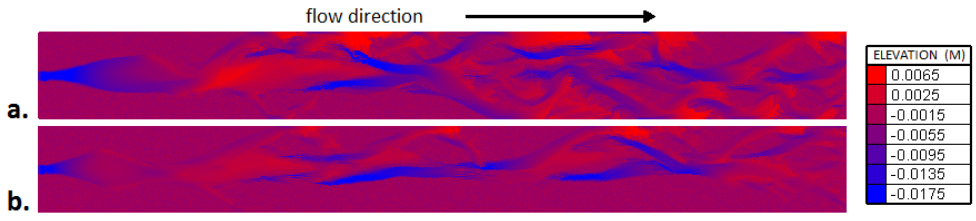

Figure 3.24: Elevation of the bed resulting after 3 hours with a. Van Rijn (1984) transport formula and b. Ashmore's (1988)

3.4.3 Widening of the domain and slope change

The widening of the domain and the slope change had the expected effects on the morphodynamics. On the one hand, the widening gave caused the water to spread. With the same flow rate as the previous

simulations, the shear stresses observed in the wide domain simulation were inferior and therefore the sediment transport low. This caused the deposition of the inflow of sediment at the entry of the domain. Although, this behavior cannot be discussed with the principle of Lane's Balance (the valley width isn't accounted of in Lane's representation), one could state that the sediment deposition at the inlet steepens the slope in order to increase the transport capacity to meet the sediment inflow.

On the other hand, the change of the slope showed that the braiding only occurred in the higher slope area, whilst the upstream low slope area was gradually steepening to adapt to the sediment inflow. The figure 3.25 shows clearly this result, which also reminds of the figure 2.4 page 13.

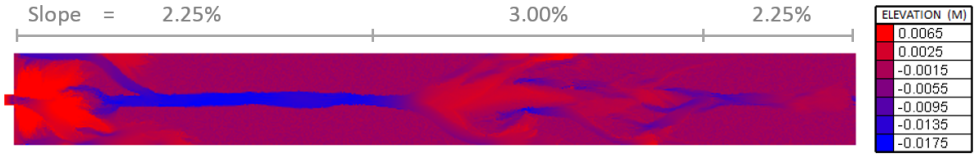

Figure 3.25: Bed's elevation. The morphological changes clearly shows the influence of the initial slope

3.4.4 Sediment grading effects

An additional run was done with consideration of bimodel sediment mixture. The material used in this model is a mixture of two sediments classes of a mean diameters of 0.65 mm and 0.95 mm. At the beginning of the simulations, the volume fraction of each sediment class is 50% and both cases are uniformly distributed in the whole domain. The global mean diameter in this case is 0.8 mm, which is the mean diameter of the uniform material considered in all the other simulations.

The classical active layer model of SISYPHE was chosen for this simulation. The active layer was considered with 1 cm thickness, which is high but helped avoiding the simulation failures due to excessive erosion in some areas. SISYPHE computes the sediment's load, and then solves the Exner equation for each class separately. The two separate evolution values are summed to give the global evolution.

The results presented in figure 3.26 showed a development of the braiding similar to the pattern resulted from uniform material model. The results also showed a rather noticeable grain sorting. The channels were usually lighter (which is the color of the coarse sediment class). However, this doesn't replicated well the observations made for the flume experiment. The grain sorting at the channels can be explained by the flushing of the fine sediments due to their high mobility. However no clear conclusion can be made regarding the model's accuracy on representing the grain sorting phenomenon.

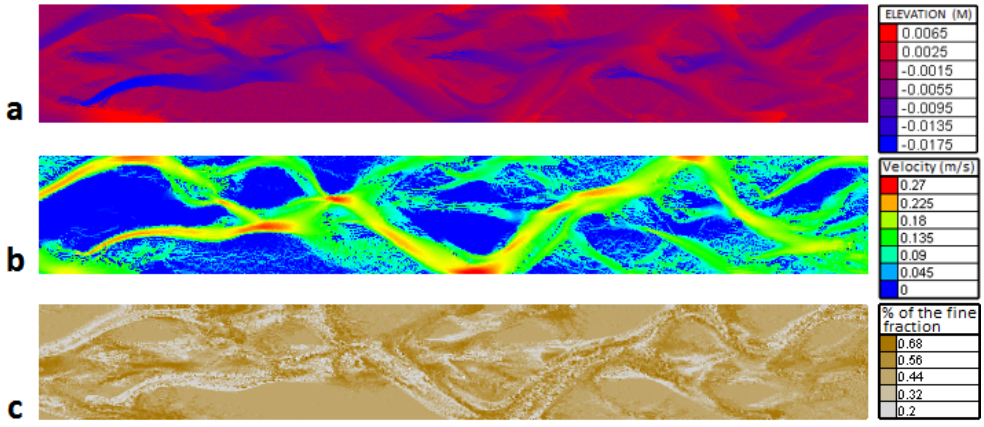

Figure 3.26: a. Bed's elevation of the bimodal material model after 3 hours, b. the velocity field, c. the grain sorting

Chapter 4

Discussion and conclusion

In this chapter, the results previously exposed will be analyzed. Indeed, the aim of the following results' discussion is to assess the accuracy of the braiding model in light of its morphometric parameters and dynamics. Consequently, the model's ability to imitate braiding streams characteristics will be discussed. Hence, conclusions regarding TELEMAC-Mascaret modeling system, or more specifically TELEMAC2D and SYSIPHE modules, as tool for the numerical modeling of braiding rivers will be discussed. These discussions will lead to the building of directions for future model's improvement and development.

4.1 Discussion of the results

First, $Run\ 0-00$ showed how the model initiated the braiding pattern. Indeed, at the beginning of the simulation, the bed starts evolving as a reaction of the hydraudynamics and sediment inflow. The results showed realistic initiation processes in agreement with flume observation as described by Leduc (2013), (Leopold and Wolman, 1957) and Ashmore (1988, 1991, 2009). However, observations of the bed evolution after 15 minutes showed the co-occurrence of the two modes and also, to some extent, the superposition of theses said modes. This was also observed in flume experiments (Chapter 3), and therefore gives a good appreciation of the model's accuracy in capturing such processes.

However, the observations on the bed's evolution, BRI, active-BRI, slopes and volumes changes agreed with the typical initiation's path of braiding streams. However, passing a certain time, the model failed in maintaining the braiding pattern and the flow gradually merged into a single channel. This behavior could be related to insufficient sediment feeding, or to inadequate representation of the processes controlling bars and bank's erosion.

The following runs, $Run\ 01$ and $Run\ 02$, investigated the effect of, respectively, the canceling of the sediment inflow and its intensification. On the one hand side, the model respond as expected to the canceling of solid feeding. A single channel, with a lower slope, and conveying all the flow rate, formed progressively from upstream to downstream. On the other hand, $Run\ 02$ didn't respond as expected. Indeed, the increase of sediment discharge didn't prevent the transformation of the active pattern into a single-thread channel.

At the end, after 13 hours, the three simulations converged to a single channel stream, each of which had a different width, sinuosity and slope. As one can foresee, the higher the sediment inflow, the steeper the main channel's slope.

Besides, the comparison of the braiding indices (Ashmore, 1991) in figure 4.1, confirmed that the models failed in sustaining the braided pattern for the three runs. The decrease of the braiding index was almost the same, and happened at the same time, regardless of the boundary conditions. This suggests

that, besides the boundary conditions, other causes are involved in the systems' tendency to converge to a single channel configuration:

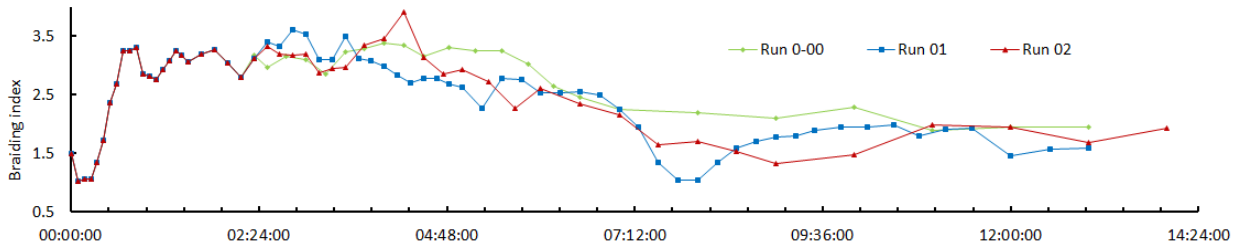

Figure 4.1: Comparison of the braiding indices (Ashmore, 1991) of the three runs

- The lack of variation of the inflow discharge;
- The unvarying inlet location;
- The insufficient refinement of the mesh as it doesn't represent well both the hydrodynamics and erosion processes near the banks.

The second part of the modeling work related to the influence of additional model's parameters. The results of the widening of the domain and the changes of its slope are rather obvious, and thus, don't need further interpretation, yet they agree with general observations of braiding rivers morphological response to the valleys topography. However, the remaining simulations gave additional insights on the model particularities.

First, the random variation of the velocities vectors' direction at the inlet nodes proved to be moderately effective in terms of sustaining the braiding pattern. This fact underlines the importance of a sustained perturbation of the flow to maintain a braiding pattern. However, as the simulation forwarded in time, the braiding was abandoned in favor of a main single channel. Also, when the flow direction was varied the braids only maintained longer, but did not evolve into another analogous braiding pattern. Which weighs in favor of the lack of representativeness of banks erosion processes as a limiting factor for braids development.

Second, the changing of the transport formula influenced the formation of braids, which developed sooner when Van Rijn bedload formula was used. For a same shear stress value, different load formulas will give different results. However, one should keep in mind the effects of the nonlinearity of sediment transport equations as stated by Recking (2013). The presented Ashmore formula has been developed with the account of the active width averaged shear stress, Meyer-Peter-Müller and Van Rijn on the basis of narrow flume experiments, whilst TELEMAC2D computes the shear stress per node. Consequently, the causes of these differences of results can be partially justified by the nonlinearity of the load equations (see figure 4.2).

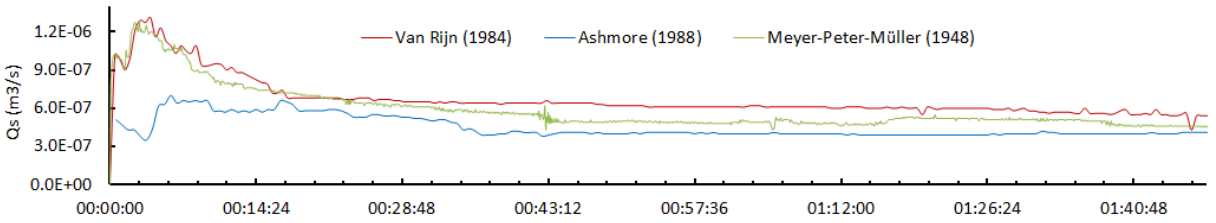

Figure 4.2: Bedload rate for the first two hours at the section *A* of the model according to different formulas

Indeed, Recking (2013) showed that such effects are even greater when the exponent of the shear stress is high. The exponents of the sear stress in Ashmore, Meyer-Peter-Müller and Van Rijn formulas are

respectively 1.37, 1.4, and 2.1. This results highlight the importance of care on the choice of transport formulas depending on the dimension of the problem, for the transition from a 1D to a 2D model will not be without consequences.

Finally, accounting of two sediments classes allowed to assess the model's ability of reproducing sediment sorting effects. Tough, some other phenomena, such as, the sliding of patches of coarse sediments and the alternate bars material sorting were observed. But, the results didn't compare well with flumes experiments' results. This might indicate a poor formulation of the grain sorting effects on the 2D module.

The discussion above showed how the model succeeded on representing the braiding initiation and, in opposition, it failed on maintaining this braiding pattern. In fact, the lack of channels dynamics was apparent and is to be attributed the models failure on sustaining dynamic and mobile braids. But, before starting the discussion of the numerical effects on the braiding evolution, it would be suitable to first recall that during the modeling work, the setting of the boundary conditions for instance, proved to be delicate task and rather limitative. In addition, in many circumstances an unrealistic and massive accumulation of sediment happened at the boundary nodes, or, exaggerated erosion/aggradation occurred in located nodes. This model instabilities compelled additional effort in the model's calibration.

In that sense, the models lack of dynamic couldn't be addressed by lowering the implication coefficient for it will deteriorate the model stability. Conversely, increasing the numerical diffusion would produce smoothed results and therefore damp, to a certain extent, the morphodynamics.

Besides, the model's stability is also conditioned by the mesh quality, which in turn impacts, not only, the CPU time, but also the results' precision. Furthermore, in a 2-D simulation the edges' length will force the minimal channel width. In fact, channels narrower than twice the distance between two nodes will not form. The small channels' (in terms of number of nodes per cross section) of evolutions is very constrained: Figure 4.3 shows the irrepresentable (in red) channel evolution and free surfaces in the case of a 3 cross nodes channel. In addition, a very high slope in a coarse 2-D mesh will cause the relative elevation of two consecutive nodes to be high, which will yield to bad interpretation of the free surface transversal profile (see figure 4.3e. and f.).

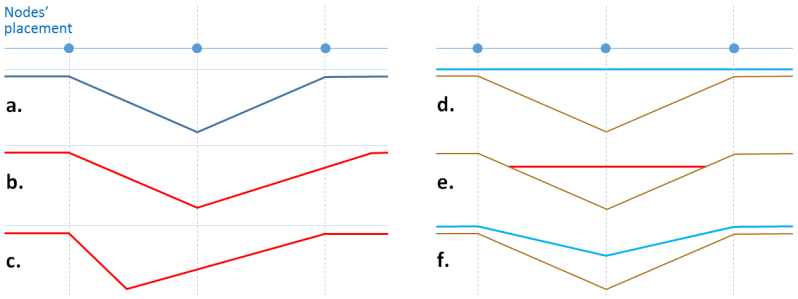

Figure 4.3: Possible (*blue*) and impossible (*red*) channels' cross sections (a., b. and c.) and the free surface (d.,e. and f.)

Which brings the discussion to the last point: the impact of mesh refinement on the representatively of the banks and therefore the impact on the bars' erosion processes.

Yet, one could first recall the observations made on the models' gradual transition to a single-thread channel in Run 00 and Run 01. The bed initially braided progressively formed a relatively wide, deep and low slope channel which carries the imposed flow rate. This conversion reminds of the observation of Tal and Paola (2010) resulting of the effects of vegetation on braiding channels in flume experiments.

Indeed, the experiments results showed that the vegetation causes the previously bare braiding pattern to transform to a meandering like stream (see figure 4.4). This transformation of the morphology is caused by the development of the plants and the ensuing effects, such as, the slowing the rate of

channels' widening and definition floodplains. The figure 4.4 emphasizes the analogous aspects of braids' transition to meander of braid due the numerical model's limitations and due to floodplain vegetation.

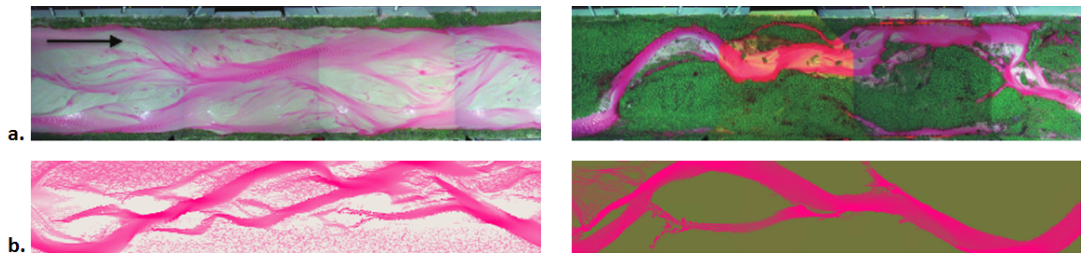

Figure 4.4: a. Transition from a braiding pattern to a single-thread channel caused by the vegetation of the floodplain (Tal and Paola, 2010), b. Similar transition observed in the Run 02 (the choice of colors only serves illustrative purposes)

In this sense, the constraint of the mesh's level of refinement as a limiting factor for small channel incision and evolution can be compared to the effects of vegetation on discouraging the reactivation channels, which is typical to braiding streams dynamics (Ashmore, 2009). This lack of braiding's dynamics was also observed in other numerical modeling studies (Schuurman et al., 2013).

Therefore, the two major limitations of the 2-D model can be related to the refinement of the mesh. However, as stated before, the number of nodes as a direct incidence on CPU efforts. Consequently, reducing the nodes spacing can make the simulation too much time consuming or even impossible. Besides, the constant refinement of the mesh can reveal to be inefficient for it will also increase the mesh definition in low interest areas. Conversely, the adaptation of the mesh to the bed's relief (close nodes in sloping areas like banks and bars' edges for instance) can reveal to be only efficient in short time scale studies since the channels pattern changes over time. The solution is therefore to have a mesh which will constantly adapt for example to the beds topography.

The figure 4.5 shows an example of an adaptive mesh. In fact, the resulting grid is refined near the banks and left coarse in relatively flat zones. Indeed, multiplying the nodes defining a bank will increase the model accuracy in these high interest regions and therefore allow a better erosion processes' representation.

In this illustrative example, first, the variation areas' detection was conducted by calculating the derivative of the bed's elevation in the transversal axis. The evolution of the bed's along the transversal axis was then used to create a density layer which assigns a high nodes' density to high variation segments and conversely, low density to the flat ones. Finally, this density layer is used to create the new adapted mesh. As one can notice, this process can easily be automatized and integrated to models. Though, the mesh generation itself is also time consuming especially in the case of triangular unstructured meshes (which proved to be favorable for the finite volume method). One should find a compromise between mesh actualization frequency and mesh maximum and minimum refinement level.

Other aspect of the mesh refinement process that should be considered with care is the choice of the threshold criterion. In the example above, the mesh refinement was linked to the variation of the topography along the cross section. This method will have the disadvantage of unnecessarily increasing the resolution even for dry undulating lands for example. Many criterions can be chosen, for instance:

- 2-D variation of the bed's elevation;
- Water depths variation;
- Velocity gradient;
- A weighted combination of this parameters;

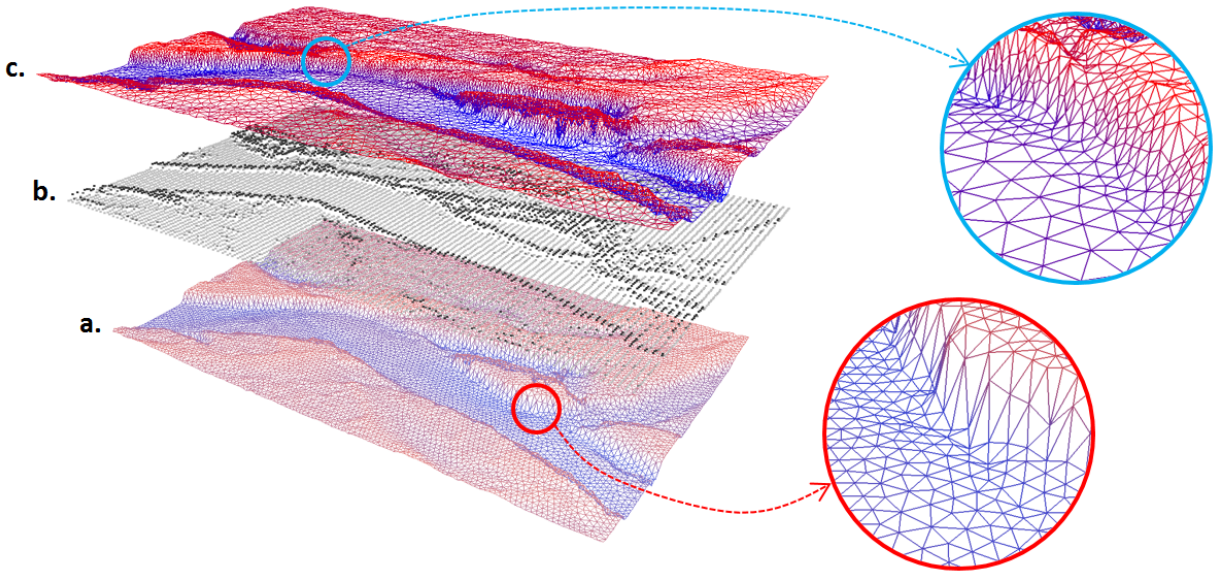

Figure 4.5: Example of mesh adaptation process. a. the initial mesh with constant nodes' spacing (9536 nodes and 18632 elements), b. the detection of high bed's variation areas, c. adapted mesh to the bed's relief with a high resolution in sloping zones (7626 nodes and 14987 elements)

4.2 Conclusion

The present report aimed at modeling the sediment dynamics in a braiding streams. To do so, a 2-D coupled hydro-sedimentary model (TELEMAC2D coupled with SISYPHE) was used. The braiding stream model was inspired from prior flume experiments. Three major cases were simulated in order to investigate the braiding formation and evolution in response to different forcings. Additional runs were done so as to broaden the assessment of the model capabilities.

The choice of working with model with a flume like dimensions model was motivated by data accessibility and availability of benchmarks in literature.

The main conclusions of this report relate to the model's ability to generate realistic braiding pattern and representing its dynamics. In that sense, the simulation results showed that the 2-D model succeeded in replicating the braiding initiation phase and the resulting pattern was presented realistic features. However, the braiding pattern didn't maintain in any of the simulations. Besides, the additional runs showed that the model reacted accurately to other forcings such as variation of the initial slope, widening of the braidplain, but failed on simulating sediments grading effect in the case of bimodal material. It also revealed that inlet perturbations improve the maintaining of braids, however, it didn't address the issue completely.

Though, one can state that most of the model's strengths mentioned above are not only specific to TELEMAC, but can also be associated to other 2-D physics based model. In fact, the success of TELEMAC on reproducing the braiding formations for example, is mostly associated to the fact that the mathematical formulations of the physical phenomena are accurate and thorough. Still, TELEMAC-Mascaret modeling, with its high flexibility and extensibility, allows benefiting from the advantages of a physical based model.

However, the main disadvantages (which can also be exported to other 2/3-D models) are, on the one hand, the high computation time. The time required for a simulation is linked to the model's time scale, the space scale, the numerical scheme and its level of refinement. Indeed, compared to other models, such as branches, neural or cellular, the general 2/3-D general models are the most time consuming. On the other hand, the uncertainties of the results are even more significant in the case of complex

pattern as the braiding rivers. As stated by Jagers (2003), a single simulation with one set of boundary conditions doesn't give enough information to speculate on a braiding river's future evolution. This last issue could be addressed by a Monte Carlo approach. Although it will multiply the computation time, it remains a promising path for future development, especially with the continual increase of computational power and the parallelization of codes.

In addition to this last TELEMAC-Mascaret modeling system development outlook, one could also add the development of a vegetation module which will account of the effect of vegetation growth on the hydro-morphodynamics. And also, the consideration of adaptive finite volume methods with a dynamic mesh with an adaptation criterion based on physical assumptions and/or error posteriori estimates.

Bibliography

Ashmore, P. (1988). Bed load transport in braided gravel-bed stream models. *Earth Surface Processes and Landforms*, 13:677–695.

Ashmore, P. (2009). Intensity and characteristic length of braided channel patternsThis paper is one of a selection of papers in this Special Issue in honour of Professor M. Selim Yalin (1925–2007). *Canadian Journal of Civil Engineering*, 36(10):1656–1666.

Ashmore, P., Bertoldi, W., and Tobias Gardner, J. (2011). Active width of gravel-bed braided rivers. *Earth Surface Processes and Landforms*, 36(11):1510–1521.

Ashmore, P. and Parker, G. (1983). Confluence scour in coarse braided streams.

Ashmore, P. E. (1991). How do gravel-bed rivers braid? *Canadian Journal of Earth Sciences*, 28(3):326–341.

Bagnold, R. A. (2008). Experiments on a gravity-free dispersion of large solid spheres in a Newtonian fluid under shear. *Proceedings of the Royal Society of London. Series A, Mathematical and Physical Sciences*, 225(1160):49–63.

Bertoldi, W., Ashmore, P., and Tubino, M. (2009). A method for estimating the mean bed load flux in braided rivers. *Geomorphology*, 103(3):330–340.

Bertoldi, W., Zanoni, L., and Tubino, M. (2010). Assessment of morphological changes induced by flow and flood pulses in a gravel bed braided river: The Tagliamento River (Italy). *Geomorphology*, 114(3):348–360.

De Linares, M. (2007). *Modelisation numérique bidimensionnelle du trasport solide et de la dynamique fluviale. Validation sur deux sites en Loire et sur l'Arc.* PhD thesis, Université Joseph Fourier, Grenoble.

Engelund, F. (1974). Flow and bed topography in channel bends. *Journal of the Hydraulics Division, American Society of Civil Engineers*, 100 , HY11:1631–1648.

Enggrob, H. G. and Tjerry, S. (1999). Simulation of morphological characteristics of a braided river. In *Proc. of the 1st IAHR Symposium on River, Coastal, and Estuarine Morphodynamics, Genova, Italy*, volume 1999, pages 585–594.

Ferguson, R. (2010). Time to abandon the Manning equation? *Earth Surface Processes and Landforms*, 35(15):1873–1876.

Ferguson, R. I. (1993). Understanding braiding processes in gravel-bed rivers: progress and unsolved problems. *Geological Society, London, Special Publications*, 75(1):73–87.

Germanoski, D. and Schumm, S. A. (1993). Changes in Braided River Morphology Resulting from Aggradation and Degradation. 101(Shen 1979):451–466.

Hervouet, J. M. (2007). *Hydrodynamics of free surface flows: modelling with the finite element method*. Wiley.

Hoey, T. B. and Sutherland, A. J. (1991). Channel morphology and bedload pulses in braided rivers: a laboratory study. *Earth Surface Processes and Landforms*, 16(5):447–462.

Jagers, H. (2003). *Modelling planform changes of braided rivers*. PhD thesis.

Lane, E. (1955). Design of stable alluvial channels. *Transactions American Society of Civil Engineers*, 120:1234–1260.

Leduc, P. (2010). Étude hydro-sédimentaire des rivières en tresses. Technical report.

Leduc, P. (2013). *Étude expérimentale de la dynamique sédimentaire des rivières en tresses*. PhD thesis, Université de Grenolble.

Leopold, L. and Wolman, M. (1957). *River channel patterns: braided, meandering, and straight*.

Malavoi, J.-R. and Bravard, J.-P. (2010). *Eléments d'hydromorphologie fluviale*.

Murray, A. and Paola, C. (1994). A cellular model of braided rivers. *Nature*, 371(Septembre):54–57.

Nanson, G. C. and Knighton, a. D. (1996). Anabranching Rivers: Their Cause, Character and Classification. *Earth Surface Processes and Landforms*, 21(3):217–239.

Piégay, H. and Grant, G. (2009). Braided river management: from assessment of river behaviour to improved sustainable development.

Recking, a. (2013). An analysis of nonlinearity effects on bed load transport prediction. *Journal of Geophysical Research: Earth Surface*, 118(3):1264–1281.

Rickenmann, D. and Recking, A. (2011). Evaluation of flow resistance in gravel-bed rivers through a large field data set. *Water Resources Research*, 47(7):22.

Rüedlinger, C. and Molnar, P. (2010). Sediment Dynamics and Morphological Change in the Braided Pfynwald Reach of the Rhone River. Technical Report March.

Schumm, S. and Khan, H. (1972). Experimental study of channel patterns. *Geological Society of America*, Bulletin 8(June):1755–1770.

Schumm, S. A. (1985). Patterns of alluvial rivers.

Schuurman, F., Marra, W. a., and Kleinhans, M. G. (2013). Physics-based modeling of large braided sand-bed rivers: Bar pattern formation, dynamics, and sensitivity. *Journal of Geophysical Research: Earth Surface*, 118(November).

Shields, A. (1936). Anwendung der Aehnlichkeitsmechanik und der Turbulenzforschung auf die Geschiebebewegung. Technical report, Preussischen Versuchsanstalt für Wasserbau.

Soulsby, R. (1997). *Dynamics of Marine Sands: A Manual for Practical Applications*. Thomas Telford Publications, London.

Tal, M. and Paola, C. (2010). Effects of vegetation on channel morphodynamics: results and insights from laboratory experiments. *Earth Surface Processes and Landforms*, 35(9):1014–1028.

Talmon, A., Struiksma, N., and Van Mierlo, M. (1995). Laboratory measurements of the direction of sediment transport on transverse alluvial-bed slopes. *Journal of Hydraulic Research*, 33(4):495–517.

Tassi, P. and Villaret, C. (2014). Sisyphe v6 . 3 User 's Manual. Technical Report 1.

Tobias Gardner, J. (2009). *Morpho-dynamics and Sedimentology of Confluences in Gravelly Braided Rivers*. PhD thesis, University of Western Ontario, London, Ontario.

Van Rijn, L. C. (1984). Sediment transport, part i: bed load transport. *Journal of Hydraulic Engineering*, 110(10):1431–1456.

Wu, W. (2008). *Computational River Dynamics*. Taylor & Francis.

Yalin, M. S. (1992). *River mechanics*. Pergamon Press.

Ziliani, L., Surian, N., Coulthard, T. J., and Tarantola, S. (2013). Reduced-complexity modeling of braided rivers: Assessing model performance by sensitivity analysis, calibration, and validation. *Journal of Geophysical Research: Earth Surface*, 118(November 2012).

Appendix A

DEM extraction with photogrammetry method

The photogrammetry method was used in order to extract the DEM of the flume experiments' braiding bed.

In the following, a short presentation of the method will be exposed, followed by a presentation of the software used and then a listing of the limitations and bias encountered.

A.1 Photogrammetry

The photogrammetry is defined as the process of precise measurements by means of photography (American Heritage Dictionary). It is used in many disciplines, such as topographic mapping, engineering, manufacturing, geology among other fields.

It principle relies on the calculation of an object's 3-D co-ordinates using 2-D images of the said object. The inputs of photogrammetric methods are the camera's orientation, the geometric parameters of the imaging process and the image co-ordinates which defines the locations of the object points' image. Some additional inputs can be accounted for such as, scale bars (to provide a scaling of the generated 3-D object), data relative to lens' distortion, etc.

In the case of this work, the multiple images of the flume were used to create a 3-D model of the sand bed and, therefore, generate a DEM of the bed's changes through time.

A.2 Agisoft Photoscan

The softer used in this work is **Agisoft PhotoScan** Professional edition. It is an advanced image-based 3-D modeling solution. Image alignment and 3-D reconstruction are fully automated (Agisfot Photoscan User Manual).

A.2.1 Principles

First, the photographs are aligned. To do so, Agisosoft Photoscan scans images to locate similar points, which will be designated by "interest points". Then, it studies the local neighborhood of each of these points (Agisoft PhotoScan – Tips and Tricks). Interest points are therefore correlates on the basis of their local neighborhood. The next step is to check, via an iterative process, and for each couple of overlapped photographs, the points' correlation with the estimated position and angle of the camera.

For instance, if two points have the same comparable neighbors (or in other terms, considered to be one same point), the camera's position and angle will determine if this two point are indeed one same point. Conversely, two akin points' matching is not validated if the camera's position contradicts this hypothesis (for example two similar points in two different unoverlapped photographs).

Second, On the basis of cameras' positions and the locations of matching points, a 3D polygon mesh is build. Once the mesh is build, Agisoft PhotoScan perfoms some correction such as closing holes in the mesh and removing detached elements.

The last step is consists on texturing the mesh. This step is not of interest for this work.

A.2.2 Results and Bias

Using Photogrammetry method, the 3-D models of the sand bed were generated at different stages of the braiding formation and evolution (see figure A.1).

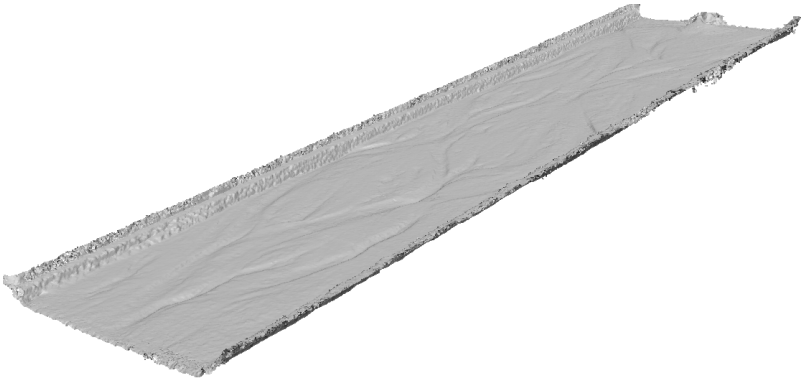

Figure A.1: 3-D model of braiding bed of the flume experiment generated by Agisoft PhotoScan

However, although the results might seem highly accurate, in most cases they were biased. Due to small lens irregularities, differences in the conditions in which the photographs were shot and small errors scaling errors, the 3-D models were more or less inaccurate.

The generated models were slightly distorted (see figure A.2), and in most cases, in an irregular manner. Indeed, the irregularities in distortions made the correction of distortions a difficult task.

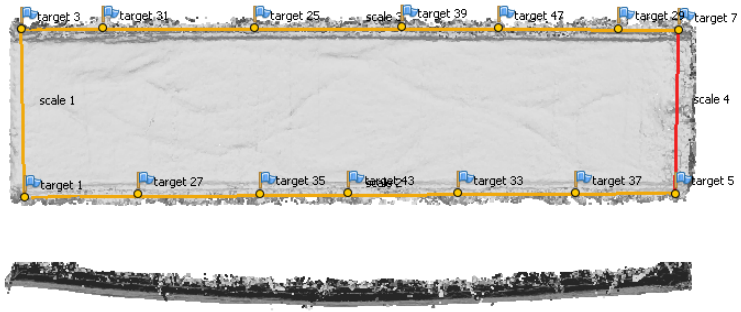

Figure A.2: Example of a distortion of the bed (the 3-D model is curved which doesn't correspond to the reality)

Besides, Agisoft Photoscan provides a distortion correction module, which readjusts the shape of the 3-D model according to the distortion parameter of camera's the lenses. Although this module helped reducing the biases, the errors remained too important. Indeed, the errors in the elevation were com-

parable to the channel depths, which made the results unsuited for mass balance analysis for instance. Even a qualitative analysis of the system evolution was tainted with these inaccuracies.

A.3 Recommendations

Digital photogrammetry is a powerful too and presents numerous advantaged compared to other DEM extraction methods. Indeed, it is relatively cheap and, to a certain extent, easy to implement.

However, as in the case of this work, the results were erroneous and couldn't be valorized. This fact, underlines the importance of following certain guidelines while taking pictures.

The user manual of Agisoft PhotoScan provides valuable a list of rules to fallow in order to get most appropriate data for 3-D model generation. However, in the following supplementary were added:

- Pictures must be as sharp as possible, which can be achieved by using a tripod and a stabilized lens;
- Lighting conditions and camera positions should remain the same in for all the runs;
- Avoid reflections and shadow zones;
- Use high quality lenses with less distortion and a high quality camera to avoid noises;
- Quantify the errors on tests in order to validate the suitability of this method to the study.

Appendix B

Steering files

B.1 TELEMAC-2D steering file

```
/-----------------------------------------------------------------------/
/       TELEMAC 2D                                                      /
/       2D modeling of braiding riviers - Flume experiments             /
/-----------------------------------------------------------------------/
/       AUTHOR  : Ismail RIFAI     DATE    : 28/04/2014                 /
/-----------------------------------------------------------------------/
/                                                                       /
/       Eight-Core Intel(R) Xeaon(R) CPU E5-2620 0 @ 2.00 GHz           /
/       4.00 Go of RAM                                                  /
/       Windows 7 Professionnel 64 bits                                 /
/       Configuration : wing64mpi                                       /
/       Compiler      : GFORTRAN 4.9.0 (GCC)                            /
/                                                                       /
/-----------------------------------------------------------------------/
/
GEOMETRY FILE                     : Maillage_4.slf
BOUNDARY CONDITIONS FILE          : t2d.cli
RESULTS FILE                      : res_t2d_sim0.slf
FORTRAN FILE                      : Subroutines.f
/
/COMPUTATION CONTINUED            : YES
/PREVIOUS COMPUTATION FILE        : res_0.slf
/
/-----------------------------------------------------------------------/
/       GENERAL INFORMATIONS                                            /
/-----------------------------------------------------------------------/
/
PARALLEL PROCESSORS                           : 8
/
VARIABLES FOR GRAPHIC PRINTOUTS               : 'H,Q,S,B,F,N'
TIME STEP                                     : 0.01
GRAPHIC PRINTOUT PERIOD                       : 5000
LISTING PRINTOUT PERIOD                       : 100
NUMBER OF TIME STEPS                          : 1080000
/
```

```
/----------------------------------------------------------------------/
/       INITIAL CONDITIONS                                             /
/----------------------------------------------------------------------/
/
INITIAL CONDITIONS                          :'CONSTANT DEPTH'
INITIAL DEPTH                               : 0.002
/
/----------------------------------------------------------------------/
/       BOUNDARY CONDITIONS                                            /
/----------------------------------------------------------------------/
/
PRESCRIBED ELEVATIONS                       : -0.177 ; 0.00
PRESCRIBED FLOWRATES                        : 0.0   ; 3.75E-4
VELOCITY PROFILES                           : 1 ; 3
/
/----------------------------------------------------------------------/
/       PHISICAL PARAMETERS                                            /
/----------------------------------------------------------------------/
/
LAW OF BOTTOM FRICTION                      : 3
FRICTION COEFFICIENT                        : 50
TURBULENCE MODEL                            : 1
/
/----------------------------------------------------------------------/
/      COUPLING WITH SISYPHE
/----------------------------------------------------------------------/
/
SISYPHE STEERING FILE  :  sis.cas
COUPLING WITH : 'SISYPHE'
COUPLING PERIOD FOR SISYPHE = 2
/
&ETA
```

B.2 SISYPHE steering file

```
/----------------------------------------------------------------------/
/       TELEMAC 2D                                                     /
/       2D modeling of braiding riviers - Flume experiments            /
/----------------------------------------------------------------------/
/       AUTHOR  : Ismail RIFAI     DATE    : 28/04/2014                /
/----------------------------------------------------------------------/
/                                                                      /
/       Eight-Core Intel(R) Xeaon(R) CPU E5-2620 0 @ 2.00 GHz          /
/       4.00 Go of RAM                                                 /
/       Windows 7 Professionnel 64 bits                                /
/       Configuration : wing64mpi                                      /
/       Compiler      : GFORTRAN 4.9.0 (GCC)                           /
/                                                                      /
/----------------------------------------------------------------------/
/
```

```
GEOMETRY FILE                    : Maillage_4.slf
BOUNDARY CONDITIONS FILE         : sis.cli
RESULTS FILE                     : res_sis_sim0.slf
/
/-----------------------------------------------------------------/
/       GENERAL INFORMATIONS                                      /
/-----------------------------------------------------------------/
/
VARIABLES FOR GRAPHIC PRINTOUTS             :'H,U,V,Q,B,E,QSBL,N,P,KS'
MASS-BALANCE                                : YES
ZERO                                        : 1e-12
SOLVER ACCURACY                             : 1.E-12
/
/-----------------------------------------------------------------/
/       BED SEDIMENT TRANSPORT                                    /
/-----------------------------------------------------------------/
/
NON COHESIVE BED POROSITY                   : 0.40
BED LOAD                                    : YES
SHIELDS PARAMETERS                          : 0.047
BED-LOAD TRANSPORT FORMULA                  : 1             / MPM
MEAN DIAMETER OF THE SEDIMENT               : 0.0008
/
/-----------------------------------------------------------------/
/       SLOPE                                                     /
/-----------------------------------------------------------------/
/
SLOPE EFFECT                                : YES
FORMULA FOR SLOPE EFFECT                    : 2             / Soulsby
FRICTION ANGLE OF THE SEDIMENT              : 30.
FORMULA FOR DEVIATION                       : 2
PARAMETER FOR DEVIATION                     : 0.85
/
/-----------------------------------------------------------------/
/  SECONDARY CURRENTS EFFECTS                                     /
/-----------------------------------------------------------------/
/
SECONDARY CURRENTS                          : YES
SECONDARY CURRENTS ALPHA COEFFICIENT        : 1.0E-00
/
/-----------------------------------------------------------------/
/  ALTERNATIVES                                                   /
/-----------------------------------------------------------------/
/
TIDAL FLATS                                 : YES
/
&ETA
```

Appendix C

Simulation results

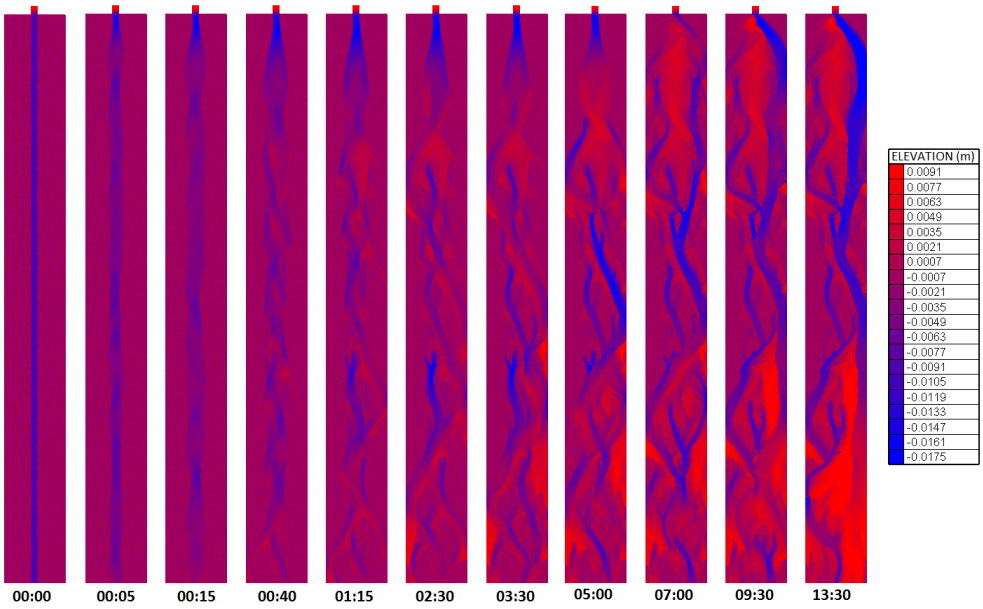

Figure C.1: *Run* 0 – 00: Bed evolution of the bed through time

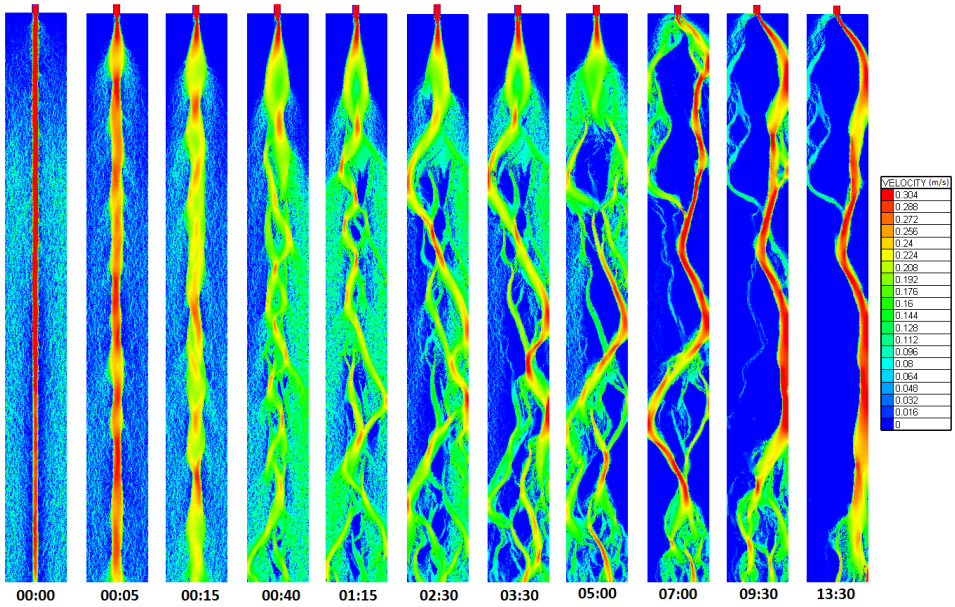

Figure C.2: *Run* 0 – 00: Flow velocity evolution through time

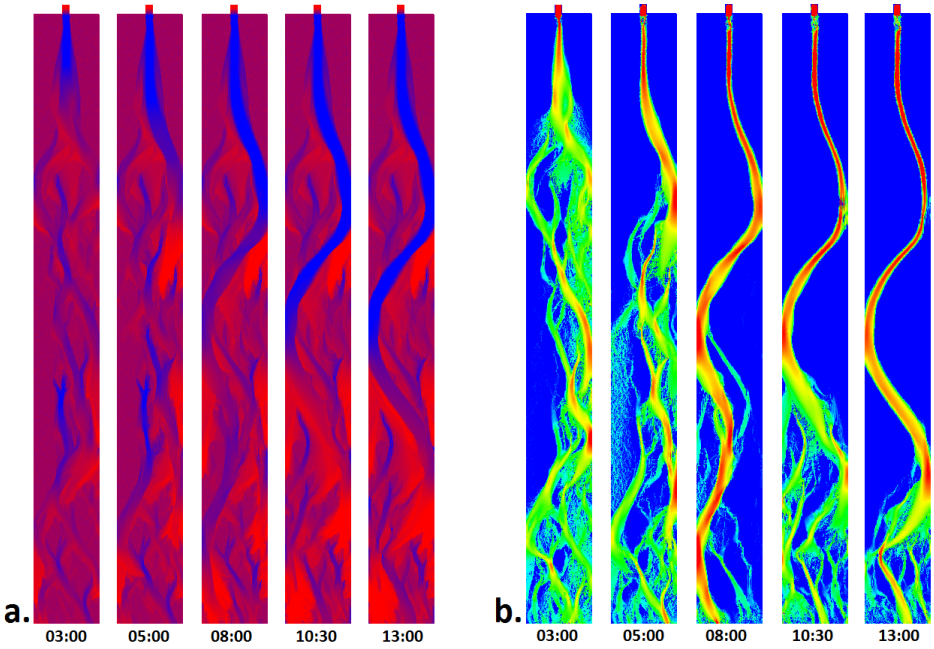

Figure C.3: *Run* 01: a. Bed evolution of the bed through time, b. Flow velocity evolution through time

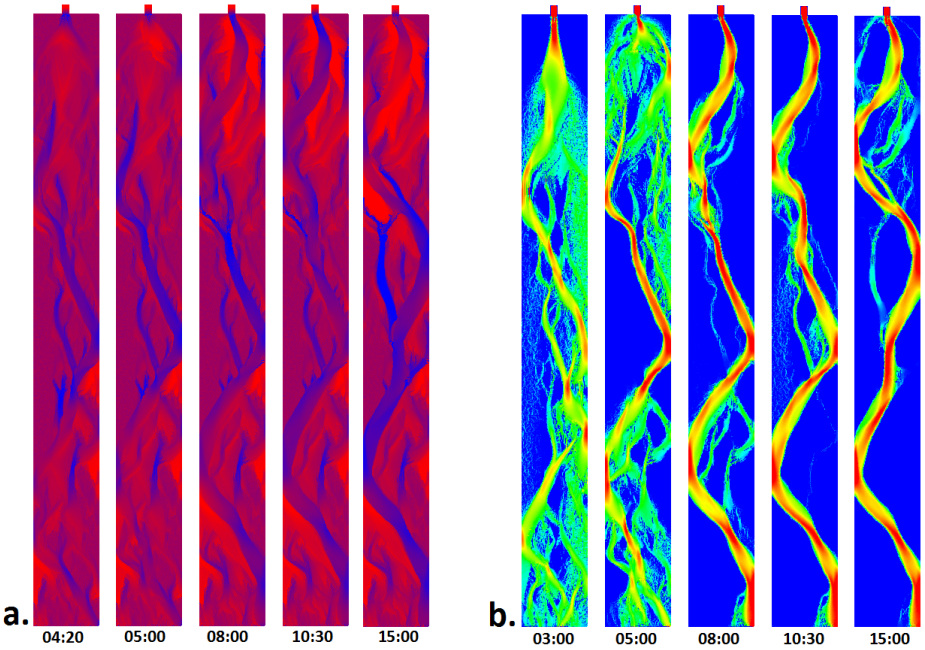

Figure C.4: *Run* 02: a. Bed evolution of the bed through time, b. Flow velocity evolution through time